

Models for Phonation

Mathematical Models for Voice Production in Nonlinear
Dynamics

Will Woolfenden

10628968

Project supervisor: Prof. Oliver Jensen

Final submission for MATH30000 Double Project for the
2022/23 academic year

School of Mathematics
The University of Manchester
United Kingdom
Saturday 13th May, 2023

Abstract

A single mass model for phonation considers steady Bernoulli flow through a channel and a vocal fold modelled by a stiff mass. The model formulates a second order non-linear ordinary differential equation for the motion of the mass with two parameters. Conditions for oscillations can be expressed in terms of the parameters involved, and we deduce explicit results involving the stationary equilibrium solutions. We formulate the equation as a first order vector ODE and derive the Jacobian matrix for equilibria, allowing us to compute eigenvalues which inform us on the stability of these stationary points. A two mass model considers the same problem with two stiffness-coupled masses and a quasisteady flow. We obtain a fourth order system with four parameters. Under strong stiffness coupling, the two masses move as one and are able to replicate the oscillatory behaviour of the single mass model. We explore parameter configurations that yield different equilibrium solutions, and again construct the Jacobian matrix to analyse the stability of these equilibrium solutions. In some cases, we can obtain results analytically. We introduce methods to verify solutions through analytical and numerical methods, and provide a Fourier analysis of particular results which yield frequency spectra of quasiperiodic motions. We end by analysing the results of the two mass model in relation to real phonation and considering how the models could be improved.

Chapter 1

Introduction

1.1 The concept and process of phonation

Phonation is a complex human mechanical process in which the vocal cords, being small regions of flexible tissue located in the larynx, begin to vibrate as air is expelled from the lungs and lower airway passages towards the throat and out of the mouth. As such, phonation can be regarded as the interaction of two processes in the body, being the exhalation of air from the lungs, and the forcing of muscles in the larynx. The extremely rich and varied tones that may be produced form the basis for the production of elongated vowel sounds.

The phonation process begins when air is expelled from the lungs. The diaphragm contracts, applying a pressure to the lungs which causes air to be driven out. Air travels through the airways, which have an extremely complicated, inverted tree-like structure, collecting in the bronchi (single airway per lung) and then trachea (single airway). Now in the upper airways, the air travels upwards from the trachea, through the larynx, and out of the body through either the nose or mouth. It is in the larynx that the mechanical process of phonation occurs. The glottis is the opening in the larynx between the vocal folds, hence the glottis must be open in order for phonation to occur. When air travels through the glottis, a decrease in pressure may cause the vocal folds to oscillate. When these oscillations occur, the propagation of the vibrations lead to the production of voiced sounds.

When the glottis closes, it may be that the vocal folds come to rest, or it could be that the glottis collapses quickly, for example in a pattern of coughing or choking. In this case, it is important to consider how the vocal folds might collapse but then rebound open again, and how this would occur. The vocal folds do not deform in a linearly elastic manner [1], meaning that the rate at which they strain is not directly proportional to the stress they are subjected to. We could imagine that on a sudden closure of the glottis, a forcing pressure from the lower airway drives the vocal folds apart again. Deformations of the vocal folds on collision are one of the features considered in “Synthesis of voiced sounds from a two-mass model of the vocal cords” [2], which will be discussed more in the section on reviewing mathematical models.

The tones produced by the oscillations of the vocal folds produce a harmonic series, which is the nature of all pitched sounds, such as those produced by musical instruments. A harmonic series, in this context, means that the waveform produced by the oscillations is a series on integer-frequency-valued periodic functions, relative to a *fundamental frequency*. Conventionally, the mathematical

definition of the harmonic series is the infinite sum:

$$\hat{W} = \sum_{n=1}^{\infty} \frac{1}{n} = 1 + \frac{1}{2} + \frac{1}{3} + \dots$$

The overtone series is the application of the harmonic series to the frequency of oscillations. If we have a fundamental frequency ω , then we can take a series of periodic functions, in this case sine, on integer multiples of the fundamental frequency. We can write this in series form as follows:

$$W(x, t) = \sum_{n=1}^{\infty} a_n \sin(ct) \sin(n\omega x).$$

For clarity, W is a function on length x and time t . The wave speed c is the speed at which the waves oscillate in time, and ω is their fundamental frequency. All frequencies $n\omega$ are integer multiples of ω . We may consider x to be bounded on an interval, such as $[0, \pi]$. In this case, we can visualise W as a series of waves on a string. The constant coefficients a_n define the weighting of the linear combination of the periodic functions. A different bias on different regions of the harmonic series lead to different textures of sound.

When formulating mathematical models, we will make several assumptions that reduce the complexity of the model, which make the process of constructing purely mathematical expressions much easier than they would be otherwise. However, these approximations and assumptions also reduce the complexity of the mathematics we derive, meaning we lose features that would arise from a model that accommodates more complex features of phonation. There are two reasons we make these assumptions. First of all, due to the scope of this project, certain features must be neglected in order to finalise mathematical relationships that we can analyse in detail. Furthermore, we want to prioritise certain aspects that we would expect to see from the model, which in this case is the oscillatory motion of the vocal cords, and hence it is reasonable to neglect features that are not directly important for this process. For example, we could neglect terms in equations if their primary importance was describing how the tension on a vocal cord affects the texture of the tone it produces, since we are not interested in terms which give extremely precise modifications to the oscillations.

1.2 Motivation

Models for phonation provide insight on the mechanics that contribute to real voice production. Humans do not have conscious control over the vocal folds, rather the muscles in the larynx work together with the exhalatory pressure from the lungs in order to induce glottal oscillations. As such, producing a model for phonation means we can begin to understand the mechanics of the process.

Our goal is to formulate a model for phonation, which we wish to can analyse to obtain mathematical descriptions of real voice production. This can be divided into several sections. First, we will briefly discuss the principles of mathematical modelling in fluid mechanics, so we have a strong foundation before building our models. When we are constructing a mathematical model, we will be able to understand how different assumptions in the basic fluid mechanics lead to different components of the model. Finally, this carries through into the analysis of the model, allowing us to make links between the results a model provides, and the mechanical properties that cause these behaviours. If we produce a model starting with only fundamental mechanics, then we can more easily understand which components of the model merit which features that arise in our analysis. This means we have clear links between the physics that forms our model, and the properties of our results.

Once we have a model, there are many directions that can be explored to develop our study, A mechanical model can act as a foundation for synthesis of speech [2], where we would apply mathematical principles of sound wave propagation. Phonation is affected by plenty of factors outside of the glottal region itself, most notably the resonance coming from the structure of the lower and upper airways as well as the mouth. The models we explore are simplified, and more generally study the properties of Bernoulli flow in wind tunnels. These have applications to the study of fluid mechanics and aerodynamics of channel flows.

1.3 Modelling phonation

As discussed, we will make limitations to the mathematical models we consider, to refine the model into something we can feasibly analyse while also gaining interesting results. First of all, while inspiratory phonation (inspiration) differs from expiratory phonation (exhalation), we will only focus on the expiratory flow case. In the construction of the model, the cases turn out to be identical up to symmetry anyway. We will also simplify the geometry of a model of the larynx, reducing the problem to the flow through a cuboid, with a vocal fold modelled by a movable wall on the side of the channel. The motion of the wall can be restricted by Hooke springs, and we can control their properties.

We will also assume either a steady or quasisteady flow. While it is entirely possible for the flow in real speech to be turbulent and not steady, assuming otherwise allows us to apply Bernoulli's equation for a steady flow, which gives a simple yet powerful statement on the relationship between pressure p , density ρ and flow velocity \mathbf{u} . Restricting our investigation to incompressible fluids, namely where ρ is constant, provides similar simplifications to our analysis.

Due to the symmetry of the vocal tract, we can simplify our analysis by only studying one side, since accommodating both sides in our model would only provide insight under asymmetric forcing terms or initial conditions.

Further assumptions we consider are the one-dimensional motion of the modelled vocal folds, the elasticity being linear and modelled by Hooke springs, and a simple geometry for the vocal tract.

1.4 Literature review for mathematical models of phonation

The paper "Synthesis of voiced sounds from a two-mass model of the vocal cords" [2, 1972] is arguably the most important work of research in the field of mathematical models for phonation. In their research, Ishizaka and Flanagan devise a two-mass model for the vocal cords, and then compute results to generate synthesised voiced sounds. The model consists of two masses to represent a vocal fold, which are stiffness coupled, comprising the wall of a channel. A flow passes through the channel and sound waves propagate from the planes, and the approximation to voiced sounds is computed as the result of the waves transmitted.

The two mass model is an extremely simple yet insightful model, which generates behaviours of seemingly erratic oscillations. The main body of this project is the formulation and analysis of a two mass model.

In the mathematical study of phonation, the myoelastic and aerodynamic theories suggest the nature of the production of voiced sounds. The myoelastic theory assumes that the vocal cords repeatedly close, each time being driven apart by the pressure from the forced airflow from the lower airways, and the frequency of this repeated process determines the frequency of the voiced sounds. The aerodynamic theory instead applies the properties of pressure in a fluid flow, imposing that a pressure drop in the glottis leads to sustained oscillations of the vocal cords. This kind of pressure

drop is often referred to as *Bernoulli pressure*, which will be discussed in more depth later. It is commonly believed that both theories are involved in the production of voiced sounds, and the ideas are discussed by Titze in “Comments on the myoelastic-aerodynamic theory of phonation” [3, 1980]. Titze is an extremely prominent author in the field of voice and hearing in mathematical modelling.

The research paper “Theory and measurement of snores” [4, 1993] involves a model which is not designed to approximate phonation. Rather, its purpose is to provide mechanical insights to the factors present in obstructive sleep apnea. However, the model itself can be applied to the investigation of phonation, being a single mass in the wall of a channel subject to stiffness and Bernoulli pressure. One of the authors, Oliver Jensen, is the supervisor for this project.

Mathematical models for the vocal folds are often heavily simplified, and hence some features of natural phonation are lost. In “Synthesis of breathy, normal, and pressed phonation using a two-mass model with a triangular glottis” [5, 2011], the authors construct a model for phonation which considers a glottis of a particular shape, which is able to close gradually. The model is able to synthesise more modes of voiced sounds than traditional models, particularly being able to produce the range of sounds from “breathy” speech (soft-spoken, close to whispering) to “pressed” (tense, thin).

1.5 Principles of fluid mechanics

Eulerian fluid mechanics in a Cartesian coordinate system defines a flow $\mathbf{u} = (u_x, u_y, u_z)$ in a 2D or 3D domain, which is a function of position $\mathbf{r} = (x, y, z)$ and time t . We will describe the 3D case. As well as a flow \mathbf{u} , we have fluid density ρ and pressure p , which are often functions of position and time. In the cases we will study, we assume the flow is incompressible, meaning ρ is uniform across the domain of the flow. This may appear like a restrictive assumption, but we still obtain rich and interesting mathematical results from the analysis of an incompressible flow.

The Eulerian framework fundamentally describes the flow field, not the fluid it contains. The change in a property \bullet of a fluid object must be found using the material derivative

$$\frac{D\bullet}{Dt} = \frac{\partial\bullet}{\partial t} + (\mathbf{u} \cdot \nabla)\bullet \quad (1.1)$$

where ∇ is the vector differential operator.

A steady flow is a flow u which is independent of time. The streamlines in a steady flow are fixed, and are identical to the paths taken by a supposed particle placed into a flow at any time. Bernoulli’s equation for a steady flow is as follows:

$$\frac{1}{2}|\mathbf{u}|^2 + \Omega + \int \frac{dp}{\rho} = \text{constant along a streamline.} \quad (1.2)$$

The term Ω is the potential for the body forces on the fluid, such as gravity. If the potential is either zero or constant, then Ω cancels when applying Bernoulli’s equation since the body forces $\mathbf{F} = \nabla\Omega$ are zero. For our research, we will assume there are no body forces and thus neglect Ω . Bernoulli’s equation is extremely useful, since it gives us a relationship between fluid velocity and pressure in a steady flow.

Fluid mass flux Q at a given cross-section is the rate at which fluid mass passes through the region, given in terms of an integral:

$$Q = - \iint_A \rho \mathbf{u} \cdot \mathbf{n} dS,$$

where \mathbf{n} is the outer unit normal to a cross-section. By convention, the outer unit normal points away from the volume, hence in the opposite direction of the flow, thus we require the negative sign. This leads to the principle of conservation of mass, where the net flux entering a volume V is the same as the rate of change of fluid mass within that volume. The net flux is the flux out minus the flow in. This can be formally expressed as follows

$$\iiint_V \frac{\partial \rho}{\partial t} dV = - \iint_A \rho \mathbf{u} \cdot \mathbf{n} dS$$

We can combine conservation of mass with the fact that for an incompressible fluid, the material derivative of density $D\rho/Dt$ is zero. We obtain an expression for incompressibility

$$\nabla \cdot \mathbf{u} = 0.$$

In this research project, the models we will consider involve simplified geometry and more straightforward assumptions of mechanics in comparison to some of the literature we have acknowledged. Fundamentally, we want to consider a fluid flow through a rigid channel, and suppose that a region of wall has freedom of motion in one dimension normal to the flow. It is appropriate to introduce the definition of a *plug flow*, being a fluid flow through a channel in which the flow is uniform over cross-sections through the channel. The plug flow model is a general form for the simple geometry channel flow models we will consider throughout this project. We will only discuss a case for a two-dimensional flow, since the intricacies are not vital to our analysis. Assume an incompressible steady flow $\mathbf{u}(x)$ travels through a channel in the positive x direction and has zero velocity in the y direction. such that the horizontal x length L of the flow is much larger than vertical y width W . We assume the flow is uniform over a cross section. We can evaluate flux over a cross-section with length/area A since velocity is uniform over said cross section, and we obtain

$$Q(x) = - \int_W \rho \mathbf{u} \cdot \mathbf{n} dS = WU \tag{1.3}$$

where $U = \mathbf{u}(x) \cdot \mathbf{e}_x$ at the point in the path of the flow normal to the cross section. The elementary vector \mathbf{e}_x is the unit vector in the positive x direction. This is assuming that the normal vector \mathbf{n} is in fact $-\mathbf{e}_x$, since this is only an example in the principle of flow in a channel. Velocity still may change in x , for example if the flow is driven by a pressure gradient in the x direction. This gives us a very flexible method to express the fluid flux in a rigid channel.

1.6 Principles of non-linear dynamics and dynamical systems

The modelling of phonation uses techniques from analysing systems of differential equations. The study of dynamical systems, as far as we are concerned, involves studying systems of differential equations that describe time-dependence in a model, and provides insight into characteristics of a model such as equilibrium solutions and classes of behaviours. In Chapter 2, we study a single mass model to approximate a vocal cord, and in Chapter 3 we generalise into a two mass model and obtain a fourth order system of differential equations. In all cases the equations of motion are autonomous and non-linear. Consider the example on two variables (x, y) , being

$$\begin{aligned} \frac{dx}{dt} &= f(x, y) \\ \frac{dy}{dt} &= g(x, y). \end{aligned} \tag{1.4}$$

In this example, the equations are autonomous, which will be the case for all problems considered in this report. The *phase portrait* is the representation in which the coordinate axes are the variables x, y , which can be generalised to higher dimensional cases, but cannot be fully visualised for dimensions higher than three. We use phase-portrait representation as an alternative visualisation of the behaviour of a system. If a variable x is governed by an ODE, we plot its behaviour over time where the different axes represent velocity dx/dt against position x , rather than just visualising position against time. The phase-portrait is a useful method of representation for problems in dynamical systems, since an ODE or system of ODEs can be characterised by the locations and properties of its stationary equilibria. This alternative approach allows us to construct visualisations that show some characteristics of a system more clearly, such as the radii of different closed orbits, and the positions of equilibrium solutions. The path we visualise in the phase portrait is a curve of the behaviour of the system parameterised by time t . Representation of solutions in the phase portrait will be vital to our analysis of our models.

If the equations f and g are non-linear, we can't do much to solve this equation. Aside from producing numerical computations, we could look intuitively for equilibrium solutions $(x, y) = (x_0, y_0)$, which are fixed point solutions for which all time derivatives of x and y are zero. Hence equilibrium solutions are equivalently solutions to the homogeneous couple $f(x, y) = 0$, $g(x, y) = 0$. Close to an equilibrium solution, we would expect the functions' behaviour to be well approximated by their first order Taylor Series approximations, being

$$\begin{aligned} f(x, y) &\approx f(x_0, y_0) + (x - x_0) \frac{\partial f}{\partial x}(x_0, y_0) + (y - y_0) \frac{\partial f}{\partial y}(x_0, y_0) \\ g(x, y) &\approx g(x_0, y_0) + (x - x_0) \frac{\partial g}{\partial x}(x_0, y_0) + (y - y_0) \frac{\partial g}{\partial y}(x_0, y_0). \end{aligned} \tag{1.5}$$

The constant terms disappear since f, g are zero at an equilibrium by definition. As $(x, y) \rightarrow (x_0, y_0)$, the terms of order $n > 1$ approach zero, and the most significant terms are those involving the first partial derivatives. We obtain the approximation for the system local to an equilibrium solution,

$$\begin{aligned} \frac{dx}{dt} &= \left(\frac{\partial f}{\partial x}(x_0, y_0) \right) (x - x_0) + \left(\frac{\partial f}{\partial y}(x_0, y_0) \right) (y - y_0) \\ \frac{dy}{dt} &= \left(\frac{\partial g}{\partial x}(x_0, y_0) \right) (x - x_0) + \left(\frac{\partial g}{\partial y}(x_0, y_0) \right) (y - y_0), \end{aligned} \tag{1.6}$$

which is a system of linear equations. For convenience, we make the substitutions $u = x - x_0$, $v = y - y_0$ which are linear substitutions proportional to the variables of interest (x, y) . Hence the above approximation is equivalent to the following matrix equation:

$$\frac{d}{dt} \begin{pmatrix} u \\ v \end{pmatrix} = \begin{bmatrix} \frac{\partial f}{\partial x}(x_0, y_0) & \frac{\partial f}{\partial y}(x_0, y_0) \\ \frac{\partial g}{\partial x}(x_0, y_0) & \frac{\partial g}{\partial y}(x_0, y_0) \end{bmatrix} \begin{pmatrix} u \\ v \end{pmatrix}. \tag{1.7}$$

Letting $\mathbf{u} = (u, v)^T$ and writing J as the matrix of derivatives, we can write the matrix equation compactly as $\dot{\mathbf{u}} = \mathbf{J}\mathbf{u}$, where the dot denotes the time derivative. The matrix \mathbf{J} is the *Jacobian matrix*. The Hartman-Grobman Theorem in dynamical systems tells us a very important result, being that the behaviour of the system near the stationary point can be determined by computing the Jacobian matrix \mathbf{J} at the equilibrium solution, and computing the eigenvalues of the matrix. The Jacobian is often a sparse matrix, and its eigenvalues are often complex-valued. For every equilibrium solution, we must compute the Jacobian and its eigenvalues in order to determine the behaviour of the system at all equilibrium points. For clarity, the eigenvalues of the Jacobian are

the constant terms λ that solve the equation $\mathbf{J} - \lambda\mathbf{I} = \mathbf{0}$, where \mathbf{I} is the appropriate size identity matrix. This also concerns the problem of finding equilibrium solutions in the first place, which is usually non-trivial. Importantly, the vector \mathbf{u} is defined on the independent variables u, v which map one-to-one to the vectors which define the phase portrait. Hence, eigenvectors of the matrix \mathbf{J} are vectors in the phase portrait from equilibrium solutions, hence they affect behaviours of the system near these stationary points.

The most important result on eigenvalues of equilibria is that an equilibrium solution is unstable if any of its eigenvalues have positive real part. Recall that the linearisation of the system is of the form

$$\dot{\mathbf{u}} = \mathbf{J}\mathbf{u}. \tag{1.8}$$

If \mathbf{J} has an eigenvalue λ for an eigenvector \mathbf{u}_0 , then we can model the trajectory from this eigenvector by the ODE and initial condition

$$\begin{aligned} \dot{\mathbf{u}} &= \lambda\mathbf{u}, \\ \mathbf{u}(t=0) &= \mathbf{u}_0. \end{aligned}$$

This is a first order vector ODE and has a general solution

$$\mathbf{u} = A\mathbf{u}_0e^{\lambda t} \tag{1.9}$$

with free scalar A . Hence the value of λ determines the trajectory from the initial point \mathbf{u}_0 . If λ has a positive real part then the trajectory diverges exponentially from the equilibrium and hence the equilibrium is unstable.

For a more rigorous understanding of the linearisation of a system of equations and an understanding of the Hartman-Grobman Theorem, see [6], particularly sections 1.1 on simple examples of linear systems, 1.5 on two-dimensional linear systems, 1.9 on the theory of stability, and 2.6 on linearisation.

1.7 Housekeeping

We will briefly discuss the notation used and any preliminary notes on methods. Within a chapter, all notation will be almost completely consistent, however variables are not consistent across separate chapters. For example, we use μ as a parameter for the single mass model, and denote eigenvalues of the Jacobian with λ , however in the two mass model we use λ as a parameter and thus it cannot be used to also denote eigenvalues, so we denote eigenvalues with σ instead.

The only significant inconsistency in our writing is when we derive the two mass model. We denote the dimensional dependent variables h_1, h_2 , and analyse the model to obtain the dimensionless variables \hat{h}_1, \hat{h}_2 . Once we have obtained the ODEs in nondimensional form, we won't consider the dimensional variables again, so for simplicity we change back to writing the independent variables as h_1, h_2 , but use them to denote the nondimensional quantities. We do the same for all the nondimensionalised variables in the problem.

The computations in this project are all performed in MATLAB, using the 64-bit double precision floating point arithmetic standard.

1.8 Structure

The first chapter of this project studies the single mass model from ‘‘Theory and measurement of snores’’ [4], which is a model formulated to consider the factors involved in obstructive sleep apnea.

We will find that the features derived in the model are very relevant to the investigation of phonation, and that this single mass model serves as a strong basis for more generalised models.

In the second chapter, we generalise the single mass model into a structure in which two masses model a single vocal cord, where the masses have a component of stiffness coupling between them. This model builds on the single mass model, but also takes strong inspiration from the two mass model formulated in “Synthesis of voiced sounds from a two-mass model of the vocal cords” [2], which discusses the formulation of a mathematical model for the purpose of generating artificial speech using a computer. The formulation and study of the two mass model is the largest and most important part of work contained in this project. After having investigated the single mass model and the two mass model, we will review the approximations and simplifications made during the formulation processes and suggest refinements to the models. We conclude by discussing the results, which are the insights to the nature of phonation that we have gained from inspecting the behaviours of the models.

Chapter 2

The single mass model

2.1 Principles of the single-mass model

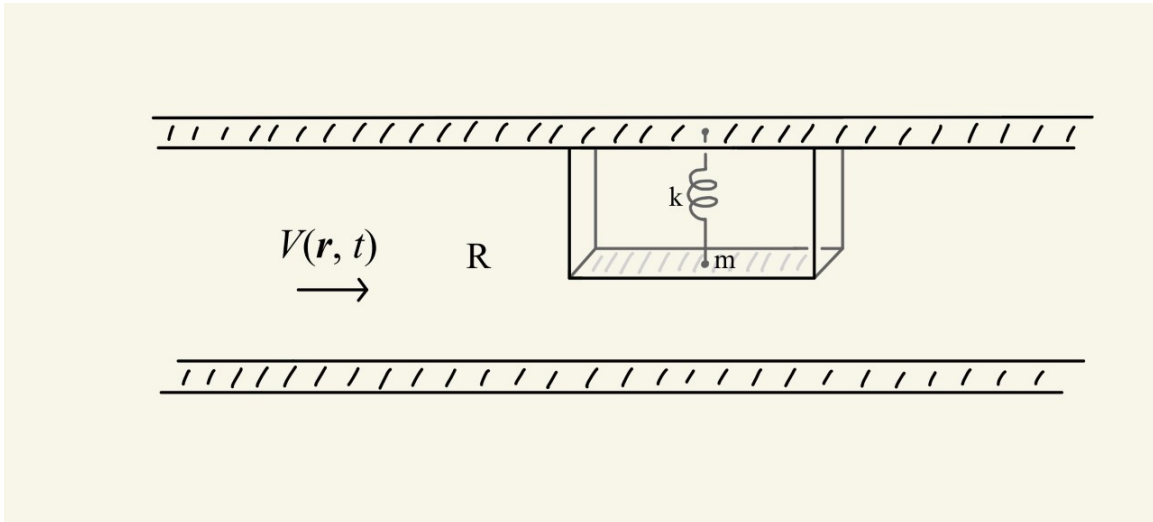


Figure 2.1: Two dimensional schematic sketch of the single mass model. Fluid flow V travels through the channel, and we are interested in the motion of the plate with mass m .

2.1.1 Derivation

The first model we will study is taken from Theory and Measurement of Snores [4]. It models the inspiratory process, designed to investigate snoring as a symptom of obstructive sleep apnea. The model proposes that the inspiratory path consists of first a region of the upper airway, which has a given viscous resistance. Then, there is a region of a channel between two walls of given area, where one wall is a suspended plate rather than being fixed in place. The term we wish to investigate is b , which describes the positive displacement between the fixed wall and the suspended wall opposite. Equivalently, b models the glottal opening. The walls themselves are assumed to

be of equal dimensions, and behave such that the surfaces are always parallel to each other. We impose that the plate may only move in the direction of b which is the normal to its surface, hence b measures the only degree of freedom of the plate's motion.

The oscillations in b that may take place, depending on conditions, is the subject of our analysis. In the original paper, the oscillations are regarded as snores, whereas here they will be regarded as the production of phones. The idea is the same, since the mathematical principles applied in the definition of the model are not exclusive in any way to particular studies of sleep apnea or the like.

Oscillations are the event where, given certain constraints, b will exhibit periodic motion, regularly returning to an initial position. In the model provided, indefinite oscillations can very much be observed given the right conditions, however it is important to be aware of some properties of the model, namely the region in which our attention is focussed. Given physical attributes are associated with the model, and so, for example, behaviours of b when negative are ignored in the investigation.

There are three forces acting on the plate in the airway, which govern the motion we are investigating. The plate is suspended in place by an elastic force F_k , namely a conventional Hooke spring with spring constant k . This spring force suspends the plate such that it resists the closure of the airway, so the tension force on the plate is acting tangent to the direction of positive displacement of the plate.

Since the upper airway has a viscous resistance R to the fluid flow, this leads to a pressure drop in the airways. An internal increase in pressure would produce an outward force on the airway, which in this model would be tangent to the positive displacement direction. Since there is instead a *decrease* in pressure, an inward force is resultant, in the direction tangent to the negative displacement. We label this force as F_p . Pressure itself is the force per unit area, so the value of the force F_p is the pressure multiplied by the surface area of the plate.

Bernoulli's equation for a steady flow gives us a relationship between pressure and fluid velocity. Assuming no body forces, the potential Ω is zero, so we can consider the flow local to the lung, and the flow near the opening. Formally, this can be represented by the equation

$$\left(\frac{1}{2}|\mathbf{u}|^2 + \int \frac{dp}{\rho}\right)\Big|_{\text{in}} = \left(\frac{1}{2}|\mathbf{u}|^2 + \int \frac{dp}{\rho}\right)\Big|_{\text{out}} \quad (2.1)$$

This expression can be rearranged to find an expression for the pressure. We would assume that the fluid velocity is zero local to the lung (in), being driven by the pressure. Hence the pressure at the opening (out) is a function of the speed local to the opening, and the forcing pressure at the lung. Note that the term $|\mathbf{u}|^2/2$ is the fluid kinetic energy per unit volume. We obtain the force F_b by multiplying this pressure term by the cross-sectional area of the plate. If this pressure is below atmospheric, then the resulting force on the plate is acting inwards, which is the same as $-F_b$ acting outwards.

The governing equation of the model is derived from Newton's second law. Given that the plate has a mass m , we know the three forces acting on it, and so the initial equation of motion can be expressed as

$$m \frac{d^2x}{dt^2} = F_e - F_p - F_b. \quad (2.2)$$

This is not the principal equation of the model, since the terms should be nondimensionalised and normalised. For example, x measures displacement but it is not stated under what scale. Furthermore, the terms for the forces are all products of pressure and their dimensional properties, meaning they measure in units that would ideally be reduced. We can normalise x by defining $b = x/x_0$, where x_0 is an equilibrium position of the plate. The forces can be nondimensionalised by dividing by the areas or volumes they are acting over. We will further explore nondimensionalisation

in the study of the two mass model. Resultingly, we produce the governing equation for the positive displacement of the channel wall from collapse at 0,

$$\frac{d^2b}{dt^2} = 1 - q - b - \frac{\mu q^2}{2b^2} \quad (2.3)$$

where μ, q are parameters linked to the properties of the fluid flow.

2.1.2 Nonlinearity

It is important to note the properties of Equation 2.3 before developing analysis. The equation itself is a second order, nonlinear, autonomous, inhomogeneous ODE. The property of nonlinearity is due to the existence of the $\mu q^2/2b^2$ term. Due to the equation being nonlinear, regular methods for solving ODEs are far less powerful, and the properties of solutions are different to regular linear ODEs. Most importantly, while linear ordinary differential equations often possess unique solutions subject to boundary or initial conditions, the same does not apply in the case of nonlinear equations.

We will first demonstrate the implications of nonlinearity by attempting methods suitable for linear ODEs, in which we do not expect to solve the ODE but instead use for demonstration. Note the absence of the db/dt term in the governing equation. We can attempt the method of reduction by proposing a substitution $v = db/dt$ and forming a first order ODE. First, note that

$$\frac{dv}{dt} = \frac{dv(b(t))}{dt} = \frac{dv}{db} \frac{db}{dt} = \frac{dv}{db} v, \quad (2.4)$$

and hence,

$$v \frac{dv}{db} = 1 - q - b - \frac{1}{2} \mu q^2 \left(\frac{1}{b^2} \right). \quad (2.5)$$

Assuming we can separate the variables, we can write an indefinite integral equation and obtain an expression for v , namely

$$\begin{aligned} \int v \, dv &= \int \left(1 - q - b - \frac{1}{2} \mu q^2 b^{-2} \right) db \\ v^2 &= \left(\frac{db}{dt} \right)^2 = 2b(1 - q) - b^2 + \mu q^2 b^{-1} + C_1, \end{aligned} \quad (2.6)$$

obtaining a constant of integration C_1 . We now have a first order differential equation on b , but this equation is even harder to reduce or even solve, as we only have the form $v^2 = g(b)$, where the first derivative is expressed explicitly but not linearly. Therefore, statements of existence and uniqueness for solutions of ODEs, which we are accustomed to, do not hold in the situation where the differential equation is non-linear.

We could have deduced this from the explicit form of Equation 2.3, but this section serves for illustration to aid the reader's understanding of why we cannot analytically solve this ODE. Additionally, the equation of the form $v^2 = g(b)$ will be useful later.

2.1.3 Properties of an autonomous system

The reader may notice that the Equation 2.3 is an autonomous ODE, namely that the independent variable t itself does not appear. If we let f be a function of b equal to the right-hand side of the equation, we can produce a plot of the behaviour of $f(b)$ against b . The visualisation of $f(b)$ shows

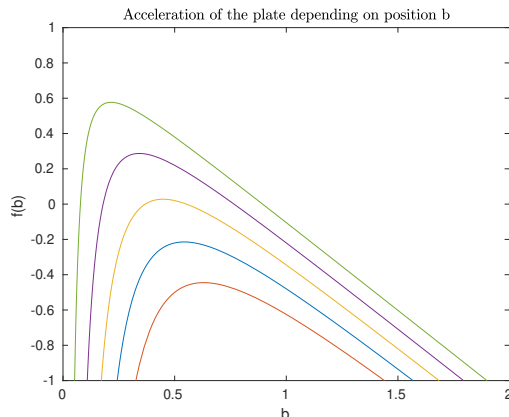


Figure 2.2: A plot of the function $f(b) = 1 - q - b - \mu q^2/2b^2$ where $\mu = 1$, q ranging from 0.1 (orange) to 0.5 (green).

the acceleration on the plate given its position. Since the equation is autonomous, f is unchanging in time. Figure 2.2 shows a plot of $f(b) = 1 - q - b - \mu q^2/2b^2$ against b .

We will introduce the concept of equilibrium solutions of the ODE, being fixed-point solutions that tell us a lot of information about the behaviour of the model. An equilibrium solution is a zero of the function $f(b)$, since all time derivatives of $b(t)$ are zero if b is fixed.

This plot allows us to deduce some intuition about the behaviour of b . At a point $b = b_0$, the function $f(b_0)$ is equal to the outward acceleration of the plate. We can see that f tends towards negative infinity both as $b \rightarrow 0$ and as $b \rightarrow \infty$, and that for certain μ, q , there is a positive region of f . Hence if b is either small or large, it will accelerate to closure, whereas for a range of intermediate values it may accelerate outwards instead. It is possible under certain conditions for b to behave similarly to a harmonic oscillator, where its position and acceleration move back and forth reciprocally.

Note that the plot of $f(b)$ does not account for velocity. Different initial conditions could cause b to behave differently under the same acceleration.

We will start by analysing the properties of the $f(b)$ curve. In order for there to exist a region of $f(b)$ that takes positive values, the local maximum of $f(b)$ must be greater than zero. We can take the derivative of $f(b)$,

$$f'(b) = -1 + \frac{\mu q^2}{b^3} \quad (2.7)$$

from which we can deduce that the maximum is located at the point where $b^3 = \mu q^2$. If we plug this back into f , we can deduce the condition

$$f((\mu q^2)^{1/3}) = 1 - q - (\mu q^2)^{1/3} - \frac{\mu q^2}{2(\mu q^2)^{2/3}} \quad (2.8)$$

$$= 1 - q - \frac{3}{2}(\mu q^2)^{1/3}. \quad (2.9)$$

We want $f((\mu q^2)^{1/3}) > 0$. We can expand and rearrange to obtain an explicit expression, being

$$\frac{(1 - q)^3}{q^2} > \frac{27}{8}\mu \quad (2.10)$$

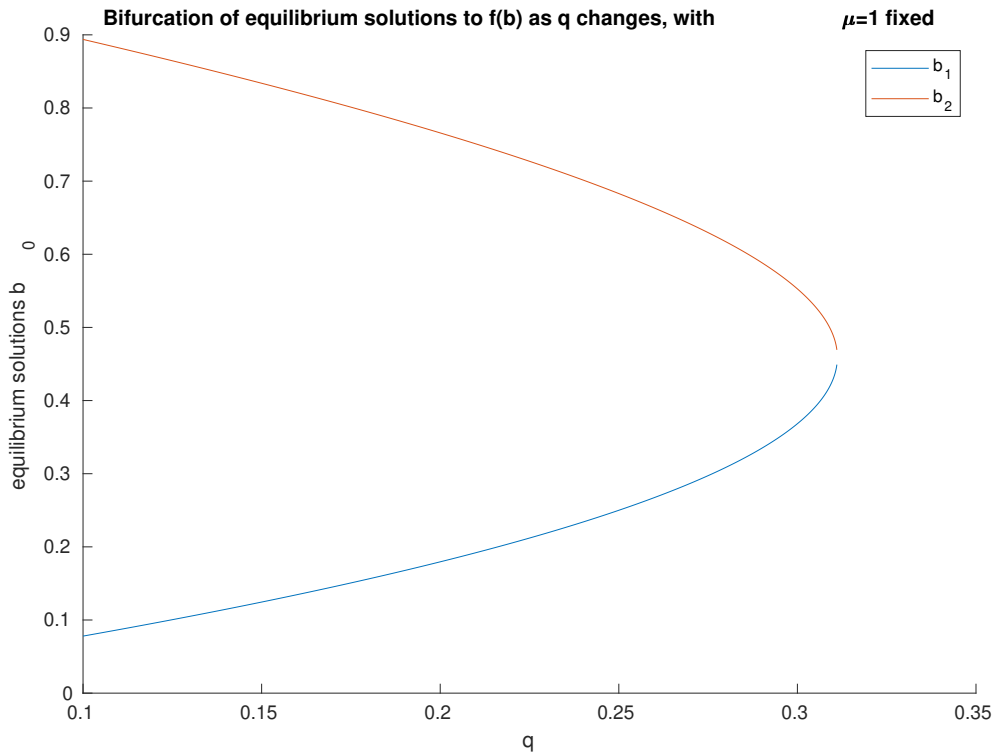


Figure 2.3: The convergence of the equilibrium solutions to a single point before annihilating. Computed by solving $f(b)$ with Newton's method. The parameter q is the independent variable that governs the distance between the equilibria, while we have μ fixed.

If Equation 2.10 is satisfied, then there exists a region of f which is positive. Hence if this condition is met then oscillations may occur. We have not yet provided the results to justify this statement, but later on we will provide more analysis on how the values of the parameters affect oscillations. Further on, we will be regularly making the assumption that this condition is satisfied, and hence that oscillations can occur, in order to develop our analysis of the model.

Equation 2.10 is a result on the existence of stationary point solutions to $f(b)$. Figure 2.3 is a plot showing the zeroes of $f(b)$ as the parameters change. With $\mu = 1$ fixed, q increases until the solutions converge close to $q = 0.3$ and annihilate. The solutions cease to exist when 2.10 is not satisfied.

We can gain interesting and useful results regarding sufficient values of μ, q , most noticeably that for any positive μ , there exists some q such that oscillations may occur. This relation is not symmetric, since $q > 1$ immediately breaks the condition, for example. It is relatively simple to deduce this, since if the $1 - q$ term of Equation 2.10 is negative, the $-3(\mu q^2)^{1/3}/2$ term will always be negative and thus the condition fails.

If a region of f is positive, and f tends to negative infinity when b approaches 0 or infinity, then there must be exactly two points b_1, b_2 which are zeroes of f . These are equilibrium solutions.

Formally, we are using the assumption of Equation 2.10 to solve

$$1 - b - q - \frac{\mu q^2}{2b^2} = 0 \quad (2.11)$$

If the acceleration of the channel wall is positive, then the wall will accelerate outwards, however the acceleration will have to oscillate from positive to negative in order for there to be oscillations in the position itself. The values of b we consider are strictly positive, since it represents a distance.

2.2 Analytical methods for the single-mass model

2.2.1 First order systems

Any ODE can be written as a system of first order ODEs. We can write Equation 2.3 in the required form as

$$\begin{aligned} \frac{db}{dt} &= \hat{b} \\ \frac{d\hat{b}}{dt} &= 1 - q - b - \frac{\mu q^2}{2b^2}. \end{aligned} \quad (2.12)$$

The variable \hat{b} is a substitute variable for the first time-derivative, such that this system is equivalent to Equation 2.3. We can write this even more compactly as a single vector-valued ODE as

$$\frac{d}{dt} \begin{pmatrix} b \\ \hat{b} \end{pmatrix} = \begin{pmatrix} \hat{b} \\ 1 - q - b - \frac{\mu q^2}{2b^2} \end{pmatrix}. \quad (2.13)$$

2.2.2 Representations of solutions and equations of motion

Oscillations are represented in the phase-plane as closed loops. It becomes easier to see the critical points, namely the stationary point in the centre of the closed loops, and the inflection point between the regions of closure and oscillation. See Figure 2.4 for a demonstration. The most common form of the phase portrait representation that we will observe in this problem is shown in subfigure B from Figure 2.4. Within a bounded region of b , closed oscillations occur, and outside of this we experience eventual closure.

Recall Equation 2.3, of the form $d^2b/dt^2 = f(b)$. Assume the right hand side $f(b)$ is the derivative (with respect to b , remaining aware that b depends on t) of some function $F(b)$. Remaining aware that b is a function itself of t , we have

$$\frac{d}{db} F(b) = f(b), \quad (2.14)$$

and if we differentiate with respect to t instead, we obtain

$$\frac{d}{dt} F(b) = \frac{dF}{db} \frac{db}{dt} = f(b) \frac{db}{dt}. \quad (2.15)$$

From Equation 2.3, we find, on multiplying both sides by db/dt and finding antiderivatives,

$$\frac{d^2b}{dt^2} \frac{db}{dt} = f(b) \frac{db}{dt} \quad (2.16)$$

$$\Rightarrow \frac{1}{2} \frac{d}{dt} \left(\frac{db}{dt} \right)^2 = \frac{d}{dt} F(b). \quad (2.17)$$

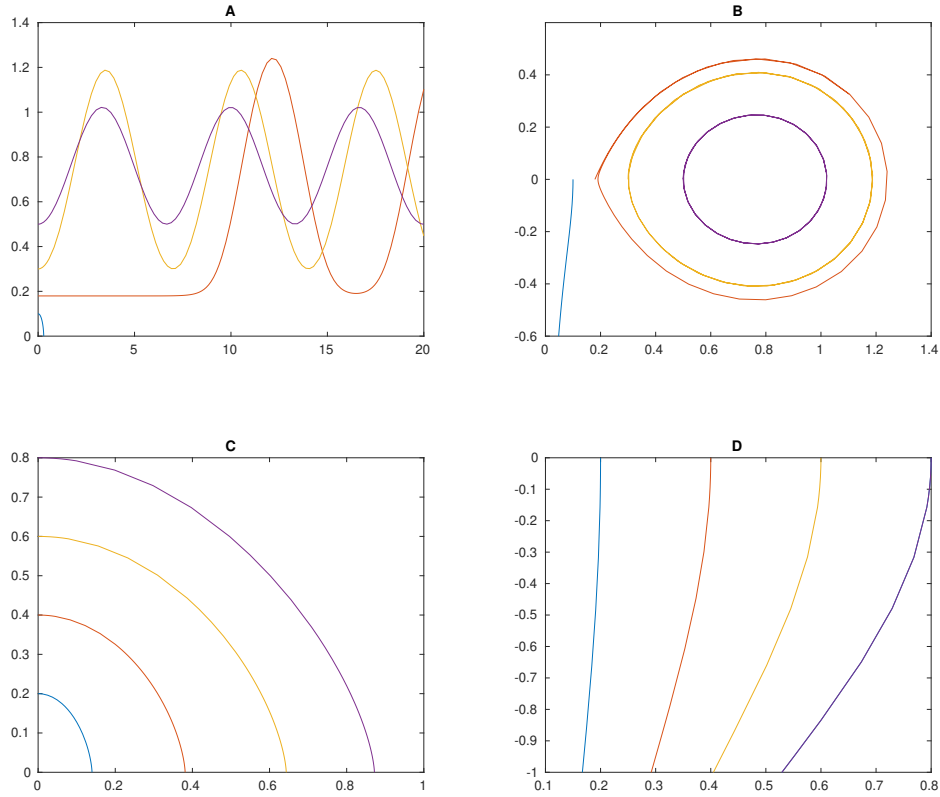


Figure 2.4: A comparison of plots in the traditional distance-time representation compared to in the phase portrait. The left column (A and C) illustrates curves as displacement against time, while the right column (B and D) draw the same plots as shown in the respective figure to the left. Figures in different rows show the model under different initial conditions and parameters. Figures A and B show the displacement b with starting positions $b = 0.1, b_1, 0.3, 0.5$, where b_1 is close to the first critical point of f . The parameters of Equation 2.3 are $\mu = 1, q = 0.2$. Figures C and D are instead computed with $\mu = 1, q = 1$ with b taking initial values $0.2, 0.4, 0.6, 0.8$. In all figures, b has zero initial starting velocity.

Integrate both sides and we obtain a result that resembles an expression for kinetic energy, namely,

$$\frac{1}{2} \left(\frac{db}{dt} \right)^2 = F(b) + C, \quad (2.18)$$

with constant of integration C . Variation of this constant leads to a family of solutions. Extremely important to note is that we have an equation in terms of $\frac{db}{dt}$ and b , which are the vectors defining the phase portrait. Hence the curves that appear in the phase portrait represent all the curves that appear for different $+C$.

Notice that Equation 2.18 is of exactly the same form as Equation 2.6, which we derived earlier. Both expressions represent families of curves in the phase-portrait. However, when reducing and solving the ODE to derive the first order reduction, we made the assumption of separability of variables, which is not true in all cases, whereas here we have covered a different method. In combination of results, we will define the function F as

$$F(b) = (1 - q)b - \frac{1}{2}b^2 + \frac{\mu q^2}{2b} \quad (2.19)$$

which is not necessarily a consistent result, as discussed in the derivation, but we will use this for verification.

We can use the plots of curves defined by Equations 2.6 and 2.18 to inspect curves in the phase portrait. For example, we can find the particular constants C such that we generate the behaviours at the critical points.

Oscillations occur when, for some C , the curve $((db/dt)^2)/2 = F(b) + C$ exhibits a closed loop. It is necessary and sufficient for there to exist a region of inflection (an interval where the derivative is positive, elsewhere negative) in $F(b)$ in order for this to occur. This is equivalent to the requirement that $f(b)$ is somewhere positive.

Interesting behaviour occurs when the local minimum or maximum of $F(b)$ is a zero. We want to investigate the integral curves to find the conditions required for

$$F(b) + C = 0. \quad (2.20)$$

If μ, q satisfy the condition for oscillations to occur, it is evident that there exists a C such that Equation 2.20 will have exactly two zeroes. The interval between these is the region in which we observe the largest oscillation.

2.2.3 The Jacobian matrix

Recall the reduction of Equation 2.3 to a first order system in Equation 2.6. Using the function $f(b)$ which we have defined, the equation can be represented by a first order system as

$$\frac{db}{dt} = \hat{b} \quad (2.21)$$

$$\frac{d\hat{b}}{dt} = f(b) \quad (2.22)$$

We can construct an approximation for the function $f(b)$ about a point b_0 using the Taylor series expansion, assuming differentiability on the variable b , of the form

$$f(b) = f(b_0) + (b - b_0)f'(b_0) + \frac{(b - b_0)^2 f''(b_0)}{2!} + \dots = \sum_{k=0}^{\infty} \frac{(b - b_0)^k f^{(k)}(b_0)}{k!} \quad (2.23)$$

Recall that $f(b)$ has zeroes. If we pick b_0 to be a zero of the function, then as $b \rightarrow b_0$, we can simplify the Taylor series expansion. More precisely, since b_0 is a zero of f , the $f(b_0)$ term tends to zero. We keep the $(b - b_0)f'(b_0)$ since, while $b - b_0$ is small, the terms succeeding it are far smaller in magnitude. With the Taylor series applied, propose the approximation about a point b_0

$$\frac{db}{dt} = \hat{b} \quad (2.24)$$

$$\frac{d\hat{b}}{dt} = (b - b_0)f'(b_0). \quad (2.25)$$

Notice that this approximation is a linear system. The obtained approximation models the ODE $b''(t) = (b - b_0)(\mu q^2/b_0^3 - 1)$. It is only valid local to points b_0 which are zeroes of f , so if $b - b_0$ grows in magnitude it is not sufficient. If we suppose a substitution of the form

$$X = b - b_0 \tag{2.26}$$

$$Y = \hat{b}, \tag{2.27}$$

then X represents the vicinity of b to b_0 , which is small, and Y is a straight substitution of the velocity value \dot{b} . We can rewrite the linear system again, this time using our substituted values

$$\frac{dX}{dt} = \frac{d}{dt} (b - b_0) = \hat{b} \tag{2.28}$$

$$\frac{dY}{dt} = \frac{d}{dt} \hat{b} = (b - b_0)f'(b_0) \tag{2.29}$$

which can be expressed as the matrix equation

$$\frac{d}{dt} \begin{pmatrix} X \\ Y \end{pmatrix} = \begin{bmatrix} 0 & 1 \\ f'(b_0) & 0 \end{bmatrix} \begin{pmatrix} X \\ Y \end{pmatrix}. \tag{2.30}$$

This is the Jacobian matrix for the ODE. The linearisation is of the form

$$\begin{aligned} \frac{dX}{dt} &= g_1(X, Y) = Y \\ \frac{dY}{dt} &= g_2(X, Y) = X f'(b_0) \end{aligned}$$

to represent the linear approximation of the ODE at an equilibrium b_0 . Then the Jacobian is the matrix of first order derivatives of X and Y ,

$$\begin{bmatrix} \frac{\partial g_1}{\partial X}(b_0) & \frac{\partial g_1}{\partial Y}(b_0) \\ \frac{\partial g_2}{\partial X}(b_0) & \frac{\partial g_2}{\partial Y}(b_0) \end{bmatrix} = \begin{bmatrix} 0 & 1 \\ f'(b_0) & 0 \end{bmatrix}, \tag{2.31}$$

which matches Equation 2.30. The characteristic polynomial for this matrix is

$$\lambda^2 - f'(b_0) = 0. \tag{2.32}$$

We have obtained the Jacobian matrix identical to how it was defined in our introduction, however the problem itself is simplified from the general form we first covered.

2.3 Computational results and further analysis

2.3.1 Formulating the problem for MATLAB

We use MATLAB, primarily the `ode45()` function, to compute solutions numerically. However, the governing differential equations must be provided as a first order system. We have explored first order forms of Equation 2.3 earlier, in Equations 2.12 and 2.13. MATLAB performs a time stepping method on a first order vector valued ODE, which is given in our case as

$$\frac{d}{dt} \begin{pmatrix} b \\ \dot{b} \end{pmatrix} = \begin{pmatrix} \dot{b} \\ f(b) \end{pmatrix}$$

By using `ode45`, MATLAB performs numerical integration on all the equations in the system, thus giving numerical solutions for b and \dot{b} in terms of time t , subject to initial conditions. In most cases, we will consider the plate moving from rest ($\dot{b}(t=0) = 0$) given an initial position $b = b_0$. All scripts are available in the appendix of this report.

2.3.2 MATLAB results and inspection

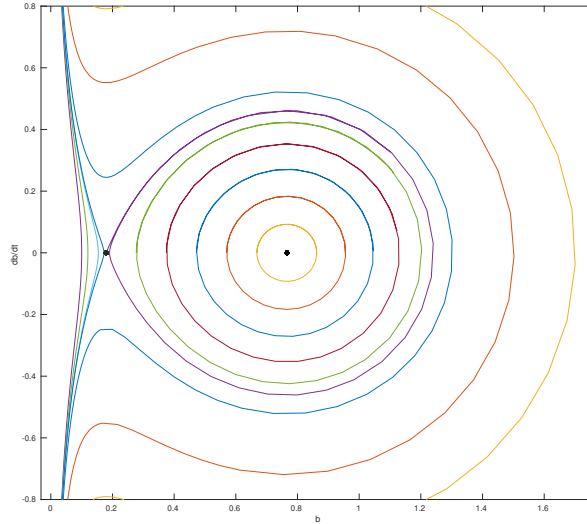


Figure 2.5: Representation of all families of curves in the phase portrait representation of numerical solutions for Equation 2.3. The parameters are set with $\mu = 1$, $q = 0.2$. The critical points were computed to be $b_1 \approx 0.1795$, $b_2 \approx 0.7659$, and have been marked.

We will first consider a range of behaviours exhibited by the model with the fixed parameters $\mu = 1, q = 0.2$, as used in subfigures A and B of Figure 2.4. Figure 2.5 is a plot showing all families of curves in the phase plane for these parameters.

We can see there are four types of curve represented. Curves that cross the horizontal axis to the left of the point b_1 represent the plate travelling and accelerating (negative velocity as the plate travels in the non-positive direction) immediately to closure. Closed loops within the enclosed region are oscillations that continue indefinitely. Curves to the right of the closed loops represent the plate also travelling towards closure, but undergoing a period of deceleration close to the critical value. This leaves two others. Two separate curves emerge directly from the point b_1 itself, however the computation is incapable of computing this path exactly when we start at zero. If we start at $b_1 + \epsilon$ where ϵ is small, the solution fails to form a closed loop that returns to its start, due to the precise behaviour of the ODE close to this critical point being subject to numerical error. Instead, this loop is shown to slightly increment the return position positively when an oscillation has been completed. The stationary point at b_2 is the oscillation with no energy, which is similar to the other closed loops.

We will compute eigenvalues of the equilibria with data to four significant figures, taking $b_1 = 0.1795$ and $b_2 = 0.7659$. We are interested in the eigenvalues of 2.30. An eigenvalue of the Jacobian is determined by the characteristic polynomial which we saw in Equation 2.32. At b_1 we have roots at $\lambda = \pm 2.4371$, which are entirely real, and at b_2 we have roots at $\lambda = \pm 0.9544i$, which are entirely imaginary. Due to one eigenvalue of b_1 having positive real part, we can deduce that b_1 is an unstable equilibrium in this case. Figure 2.8 shows the equilibrium solutions as the parameter q changes and plots their eigenvalues in the complex plane as the equilibrium solutions converge.

In the proximity of b_2 , oscillations can be observed about the fixed point, but in proximity to

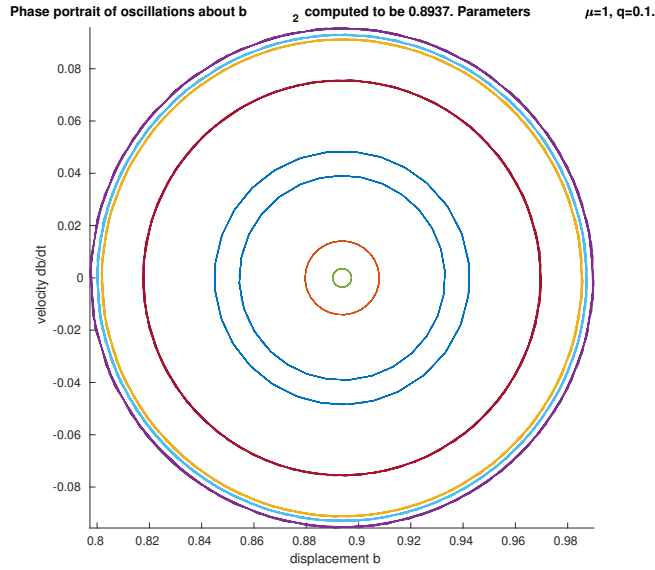


Figure 2.6: Oscillations about the equilibrium solution b_2 with parameters $\mu = 1$, $q = 0.1$, represented in the phase portrait. Computed using a random angle and small modulus to offset initial conditions within a small disc about b_2 in the phase-plane. We always observe regular oscillations that continue indefinitely.

b_1 we can observe a variety of behaviours. Figures 2.6 and 2.7 show the behaviours local to each equilibrium solution. We conclude that if the Jacobian has entirely real eigenvalues at a stationary point, it is unstable, whereas if the eigenvalues are entirely imaginary (complex with zero real part) then it is stable.

Clearly in order for a stationary point b_0 to have real eigenvalues, we must have $f'(b_0) \geq 0$ such that the characteristic polynomial has real roots. If $f'(b_0) = 0$, eigenvalues will be zero since \mathbf{J} is not a full-rank matrix. This condition can be expanded and written more explicitly as $\mu q^2 \geq b_0^3$, which is a surprisingly simple expression.

In any case where the curve f has exactly two zeroes for positive b , we can compute these points and the eigenvalues of the Jacobian at each. If the curve f has, instead, exactly one zero for positive b , then the curve $F(b)$ has a point of inflection, but its gradient (f itself, by definition) is always negative. We require equality in Equation 2.10 for any suitable parameters, which can be rearranged into the form

$$27\mu q^2 = 8(1 - q)^3. \quad (2.33)$$

We have no restrictions on uniqueness of solutions to this equation. Suitable real rational values for μ, q are $\mu = 64/81, q = 1/3$. Real rational solutions allow us to solve this case analytically. The

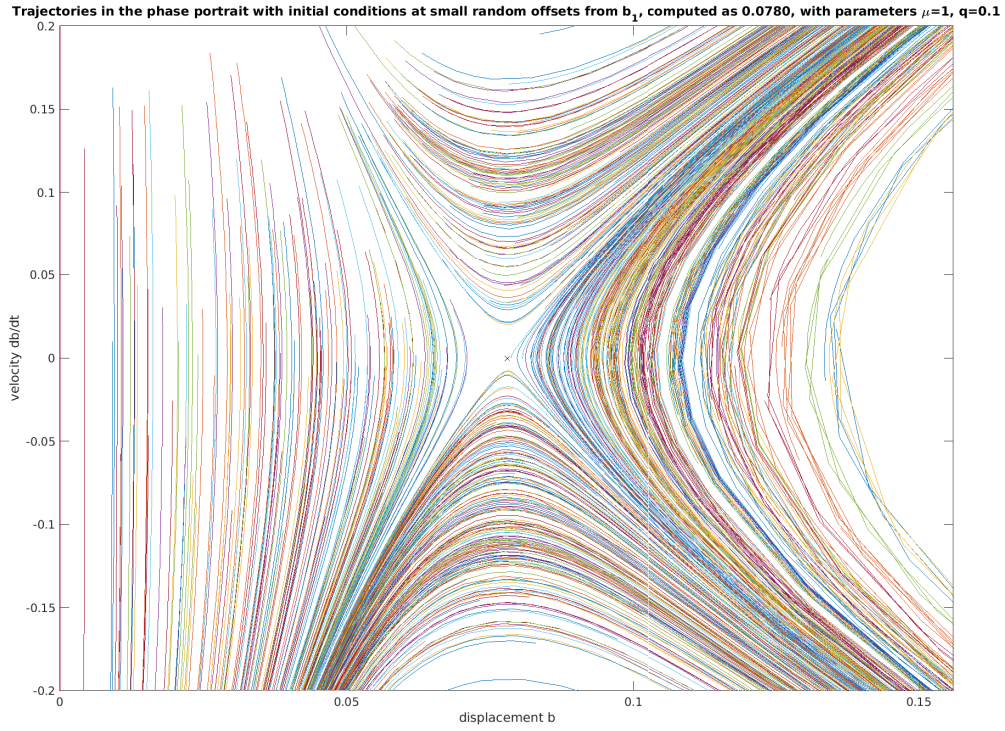


Figure 2.7: Trajectories about the equilibrium solution b_1 with parameters $\mu = 1, q = 0.1$, drawn in the phase portrait. Paths either accelerate to closure (left of the fixed point), fall into orbit about b_2 (right), or follow a path outside of the closed region of oscillations (top and bottom) before closure. We view an extremely close image of the unstable point, showing how oscillations (right of the stationary point) come extremely close to the equilibrium.

single equilibrium is $b_0 = (\mu q^2)^{1/3} = 2^2/3^{5/3}$. We can solve the eigenvalue equation as follows

$$\begin{aligned} \det(\mathbf{J} - \lambda \mathbf{I}) &= 0 \\ \lambda^2 - f'(b_0) &= 0 \\ \lambda^2 - f'((\mu q^2)^{1/3}) &= 0 \\ \lambda^2 + 1 - \frac{\mu q^2}{(\mu q^2)^{1/3}} &= 0 \\ \lambda^2 + 1 - (\mu q^2)^{2/3} &= 0 \\ \lambda^2 + 1 - \frac{2^4}{3^{10/3}} &= 0 \\ \lambda^2 &= \frac{2^4}{3^{10/3}} - 1 \\ \lambda &= \pm \sqrt{\frac{2^4}{3^{10/3}} - 1} \\ \lambda &\approx \pm 0.7675i \end{aligned}$$

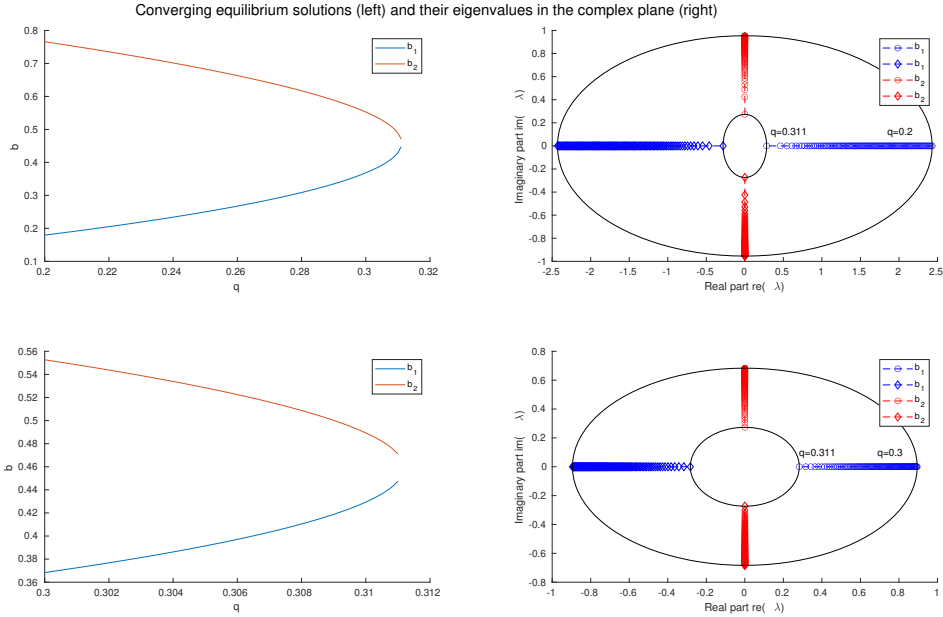


Figure 2.8: Equilibrium solutions (left) of f for fixed $\mu = 1$ as q changes, and eigenvalues of the Jacobian matrix (right) as the solutions change. The eigenvalues in the right figures are always pairs up to sign, since the equation involves the determinant of the 2×2 Jacobian matrix. The eigenvalues of b_1 are always entirely real, while the eigenvalues of b_2 are always entirely imaginary. Ellipsoids are rendered to mark the moduli of the eigenvalues for different values of q .

hence at the single equilibrium, the eigenvalues are entirely imaginary, similar to the b_2 equilibrium in the particular case we computed earlier.

2.3.3 Comparison to analytical results

The region of initial b , with zero initial velocity, for which oscillations will occur, is computed to be the approximate interval $(0.18, 1.24)$. We will assume Equation 2.19. If the integration constant satisfies $C = -F(b_1)$, then the curve has exactly two positive zeroes: one being at $b = b_1$ and the other where $b > b_2$ as the curve crosses the horizontal axis as it tends to negative infinity. This means the curve $F(b)$ is also zero at the stationary point $b = b_1$. Hence the range of zeroes to verify results should be the solutions to the equation $F(b) - F(b_1) = 0$, in full

$$(1 - q)b - \frac{1}{2}b^2 + \frac{\mu q^2}{2b} - F(b_1) = 0. \quad (2.34)$$

This is guaranteed to be zero at $b_1 \approx 0.1795$. We have the parameters $\mu = 1$, $q = 0.2$

We are more interested in whether or not the other end point of the interval is consistent. The function $F(b) + C$ draws curves in the phase portrait. We want to consider oscillations, which require

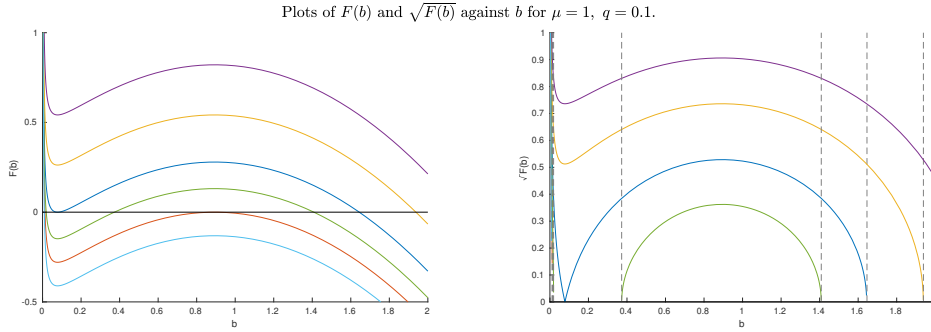


Figure 2.9: Plots of $F(b) + C$ and $\sqrt{F(b) + C}$ against b . The right-hand-side plot resembles the plots of the model's behaviour in the phase portrait, since Equation 2.18 gives us a relationship between the two.

solutions to the equation

$$F(b) + C = (1 - q)b - \frac{1}{2}b^2 + \frac{\mu q^2}{2b} + C = 0. \quad (2.35)$$

It is fairly simple to figure out that if $F(b) + C = 0$ is required at the stationary point b_1 , then $C = -F(b_1)$. The function $F(b) - F(b_i)$ is zero at b_i , allowing us to construct functions representing the kinetic energies of a solution to the ODE, which take zero at the equilibrium solutions.

Figure 2.9 shows plots of $F(b) + C$ and $\sqrt{F(b) + C}$ for different constants C . The blue curve is the line $F(b) - F(b_1)$ at the stationary point b_1 , and plotting its square root forms a sharp point where it intersects with the horizontal axis. This resembles the shape of the unstable equilibrium in the phase portrait, which we visualised in Figure 2.7.

We will now show that Equation 2.10 guarantees oscillations. Assume that $f(b)$ is somewhere strictly positive, which is equivalent to 2.10. We do not include the case of equality, which is where $f(b)$ is zero exactly once. Equivalently, $F(b)$ has a region of inflection, since its gradient $f(b)$ is positive on a given interval. As shown by Figure 2.9, the curve $F(b) - F(b_1)$ is equivalent to the closed loop in the phase portrait that starts and ends at b_1 . Curves $F(b) - F(b_1) - \eta$, where η is small, correspond to closed loops bounded by the curve $F(b) - F(b_1)$. For sufficiently small η such that $b_1 + \eta$ is contained between the zeroes of $F(b) - F(b_1)$, we have a closed loop, which corresponds to an orbit represented in the phase portrait.

2.4 Review and motivation

The single mass model is capable of producing oscillations within a bounded region. Trajectories converge towards the vicinity of the unstable equilibrium when they pass near the boundary for oscillations. Close to the stable equilibrium, oscillations are periodic and regular. However, the motions of the mass have a very simple pattern which do not relate very strongly to the complicated nature of the mechanics of phonation. We will develop a two mass model, using the concepts we have introduced so far, for a further study.

Chapter 3

The two mass model

3.1 Formulating the model

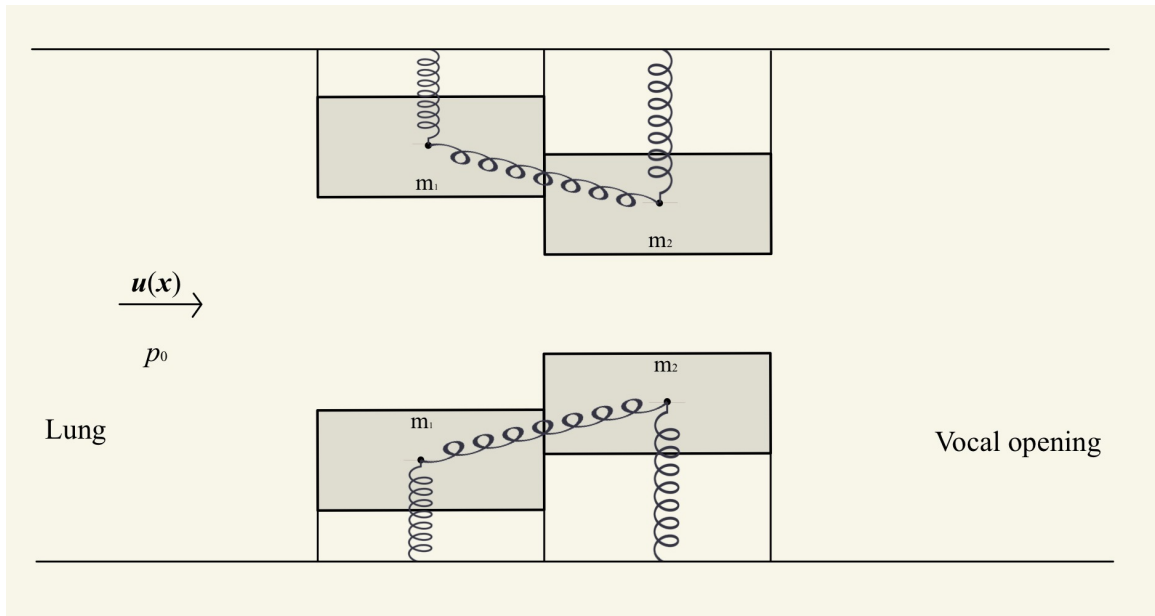


Figure 3.1: General illustration of the two mass model. Plates with mass m_1, m_2 are connected to the wall of the channel by springs. The fluid velocity \mathbf{u} and pressure p are terms we can fix local to the lung. The stiffness coupling between masses provides a horizontal force which we ignore by restricting the masses to one-dimensional motion along the width of the channel.

We will begin to construct a model for phonation involving two stiffness-coupled masses. Due to symmetry, we will only consider one side of the channel. We consider a steady flow \mathbf{u} passing through a channel, in which two masses cause a constriction to the fluid passage. Each mass m_j is individually supported by a spring with Hooke constant k_j , and a coupling spring with constant k_s connects the two masses.

3.1.1 Fluid and solid mechanics

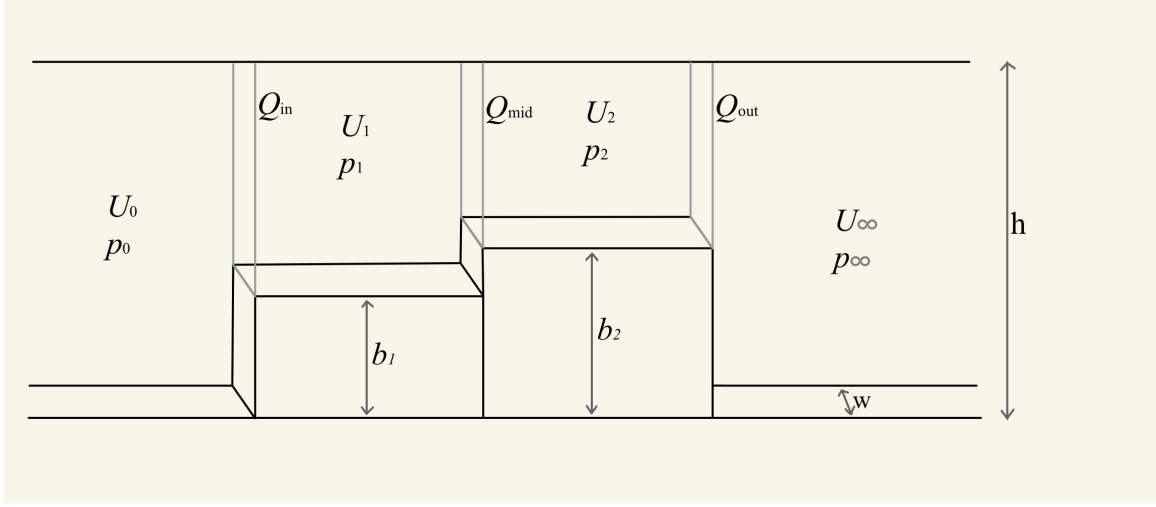


Figure 3.2: The single side of the model. Flux Q is of interest on the boundaries between masses, and we can use flux to either deduce or assume relationships involving pressure and fluid velocity.

3.1.2 Modelling with unknown flux

The two mass model considers a quasisteady flow in order to simplify the relationships that determine the fluxes at different points in the structure. However, we will first discuss a full formulation without this assumption.

We assume that each mass moves one-dimensionally in the direction perpendicular to the dominant flow. The extruding motion of each mass j into the channel is given by b_j . The masses may close to $b_j = h$ at closure, or extend outwards (increasingly negative b_j) indefinitely. We assume an incompressible fluid travels in a plug flow, which neglects the possibility of any stagnation or interference. In the introduction we defined the concept of flux, however now we divide by ρ to give the total flow per unit volume that travels across a cross section. With a pressure driven flow, we can fix p_0 and U_0 , being the fluid pressure and velocity local to the lung (at x_0). Hence, we can evaluate the flux $Q_0 = Q(x = x_0)$ at the lung

$$Q_0 = - \iint_{A_0} \mathbf{u}(x_0) \cdot \mathbf{n}(x_0) \, dS. \quad (3.1)$$

since the velocity at x_0 is scalar U_0 in the positive x direction, this becomes

$$Q_0 = \iint_{A_0} U_0 \, dS = whU_0 \quad (3.2)$$

where wh is the area of A_0 . Since we have changing volumes, we can still maintain conservation of mass without requiring uniform flux across the whole model. In the glottal region we have flux Q_{in} on the entry border of the two mass region, and Q_{out} on the exit, with Q_{mid} on the plane in between the masses. The regions before and beyond the glottal opening are fixed channels, hence the flux

is consistent in these regions and we can state that $Q_{\text{in}} = Q_0$ and $Q_{\text{out}} = Q_\infty$. We then find the velocities from the flux, by dividing by the area of the cross section

$$\begin{aligned} U_{\text{in}} &= \frac{Q_{\text{in}}}{wh_1} \\ U_{\text{out}} &= \frac{Q_{\text{out}}}{wh_2}, \end{aligned} \tag{3.3}$$

which gives us the fluid velocities on the borders of the glottal region. However, in order to find the fluid velocity in the two glottal volumes, we need some kind of interpolatory flux. We will make the assumption that the fluid velocities in their respective volumes are determined by the flux, where we take the average flux using the borders of each region:

$$\begin{aligned} U_1 &= \frac{1}{wh_1} \left(\frac{Q_{\text{in}} + Q_{\text{mid}}}{2} \right) \\ U_2 &= \frac{1}{wh_2} \left(\frac{Q_{\text{mid}} + Q_{\text{out}}}{2} \right). \end{aligned} \tag{3.4}$$

We can directly express a relationship between the change in the size of a volume and the change in the volume of fluid that enters that region. First, the two glottal volumes V_j have dimensions $h_j wd$ where $h_j + b_j = h$ for $j = 1, 2$. Since h_j is the only dimension which is not fixed, we can take time derivatives:

$$\dot{V}_j = \dot{h}_j wd. \tag{3.5}$$

The dot denotes explicit time derivative. We can write these in terms of the net flux, being flux in minus flux out, in each volume

$$\begin{aligned} \dot{h}_1 wd &= Q_{\text{in}} - Q_{\text{mid}} \\ \dot{h}_2 wd &= Q_{\text{mid}} - Q_{\text{out}}. \end{aligned} \tag{3.6}$$

We have deduced several properties of the velocity of the fluid through different locations in the model, however we don't have explicit expressions for either the plate velocities or the fluxes, which are the key values in our problem.

3.1.3 Quasisteady flow

We will now introduce the assumption of a quasisteady flow. In this simplification, we have a constant flux Q throughout the structure, which makes it easier to find the pressure terms that we are interested in. In turn, we lose a lot of powerful statements from earlier. For example, Equation 3.6 is trivialised since the fluxes cancel. We will continue our formulation of the problem, retaining that the fluid is incompressible and driven by the forcing pressure p_0 from the lung. Recall Bernoulli's equation for a steady flow. In order to evaluate an expression for the pressure in a region, we need to know the fluid velocity, the body forces, and the local density. Fortunately we have assumed incompressibility, so the density ρ is constant, and we choose to neglect body forces.

Along a streamline, we have:

$$\begin{aligned}
\frac{1}{2}\rho U_0^2 + \tilde{p}_0 &= \rho E && \text{(lower airway)} \\
\frac{1}{2}\rho U_1^2 + \tilde{p}_1 &= \rho E && \text{(volume } V_1) \\
\frac{1}{2}\rho U_2^2 + \tilde{p}_2 &= \rho E && \text{(volume } V_2) \\
\frac{1}{2}\rho U_\infty^2 + \tilde{p}_\infty &= \rho E && \text{(upper airway),}
\end{aligned} \tag{3.7}$$

where E is the Bernoulli constant on the streamline. We can rearrange and obtain explicit expressions for pressure, being

$$\begin{aligned}
\tilde{p}_0 &= \rho \left(E - \frac{1}{2}U_0^2 \right) \\
\tilde{p}_1 &= \rho \left(E - \frac{1}{2}U_1^2 \right) \\
\tilde{p}_2 &= \rho \left(E - \frac{1}{2}U_2^2 \right) \\
\tilde{p}_\infty &= \rho \left(E - \frac{1}{2}U_\infty^2 \right).
\end{aligned} \tag{3.8}$$

In the upper airway we have \tilde{p}_∞ local to the vocal opening, hence this is *atmospheric pressure*, which we will write as \tilde{p} . If we have zero fluid velocity local to the lung, and the fluid is driven by the pressure, we have that $\tilde{p}_0 = \rho E$, and if \tilde{p}_∞ is atmospheric pressure, then $\rho(E - U_\infty^2/2) = 0$ In combination:

$$\tilde{p}_0 = \rho E = \frac{\rho U_\infty^2}{2} \tag{3.9}$$

In the regions of interest, we are concerned with the difference in pressure from atmospheric level, which are the pressure values we actually wish to compute. We express the pressure terms as follows:

$$\begin{aligned}
p_0 &= \rho E - \rho \frac{1}{2}U_0^2 - \rho E + \rho \frac{1}{2}U_\infty^2 = \frac{1}{2}\rho (U_\infty^2 - U_0^2) \\
p_1 &= \frac{1}{2}\rho (U_\infty^2 - U_1^2) \\
p_2 &= \frac{1}{2}\rho (U_\infty^2 - U_2^2).
\end{aligned} \tag{3.10}$$

Importantly $p_0 = \tilde{p}_0$ is still the forcing term.

In a quasisteady flow, we can deduce velocities using the uniform flux Q . Equation 3.6 gave us an expression for velocity in terms of flux and the channel dimensions, which we can generalise outside the region of interest:

$$U = \frac{Q}{wh}, \tag{3.11}$$

and in a region of interest we use the variable channel height instead

$$U_j = \frac{Q}{wh_j} \tag{3.12}$$

for $j = 1, 2$.

We now have a construction for pressure in terms of the plate displacement, thus can write the pressure-induced force on the plate. Given $j = 1, 2$:

$$\begin{aligned}
 p_j &= \rho \left(E - \frac{1}{2} U_j^2 \right) \\
 &= \frac{1}{2} \rho (U_\infty^2 - U_j^2) \\
 &= \frac{1}{2} \rho \left(\left(\frac{Q}{wh} \right)^2 - \left(\frac{Q}{wh_j} \right)^2 \right) \\
 &= \frac{\rho Q^2}{2w^2} \left(\frac{1}{h^2} - \frac{1}{h_j^2} \right).
 \end{aligned} \tag{3.13}$$

We can multiply the pressure p_j by the area $w d$ of plate j to find the force.

3.1.4 Forming the equations of motion

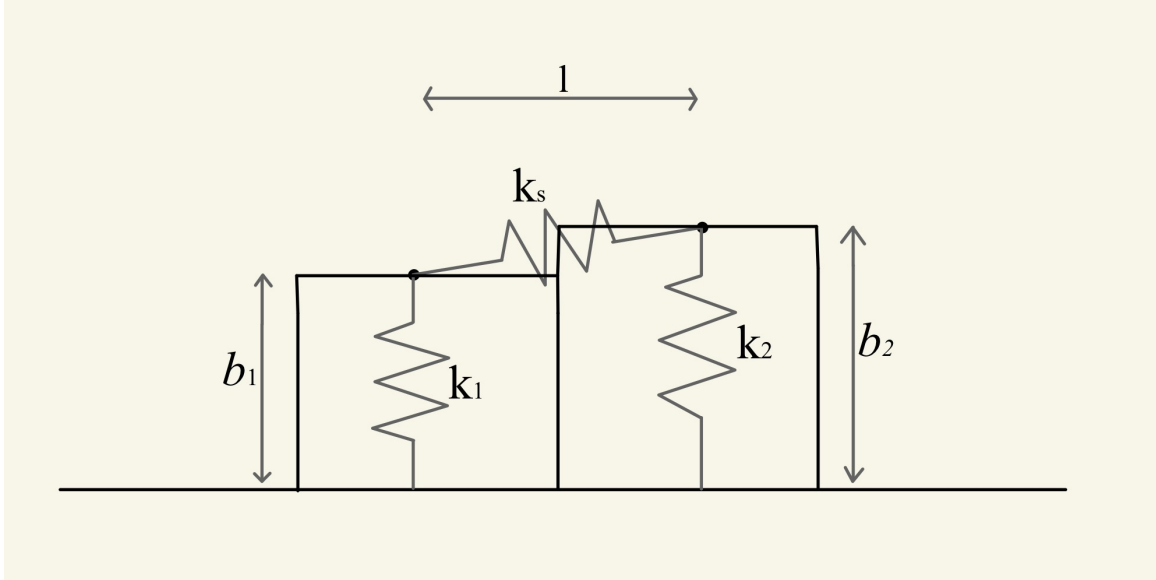


Figure 3.3: Illustration of the lengths b_1, b_2 and the springs connected to the masses. The springs connected to the wall act as support, preventing the Bernoulli pressure drop from forcing the walls into closure similarly to the single mass model. The coupling spring provides a stiffness such that the two masses can be thought of as one body consisting of two components. The springs allow us to deduce forces acting on the masses which stimulate motion by Newton's second law.

We use linear elastic Hooke springs to model the stiffness of the walls. Support springs are similar to the original model we have considered, however we now introduce stiffness coupling between two separate walls. A plate $j = 1, 2$ is connected to the wall by a stiffness spring with constant k_j . The coupling spring has constant k_s , and the resting equilibrium positions of all springs are at $b_j = 0$.

The forces on a plate with position b_j provide the equation of motion by Newton's second law:

$$m_j \frac{d^2 b_j}{dt^2} = -F_{\text{stiffness}} - F_{\text{pressure}} + F_{\text{coupling}} \quad (3.14)$$

for $j = 1, 2$. In full:

$$\begin{aligned} m_1 \frac{d^2 b_1}{dt^2} &= -k_1(b_1 - b^*) - \frac{wd\rho Q^2}{2w^2} \left(\frac{1}{h^2} - \frac{1}{(h - b_1)^2} \right) + k_s(b_2 - b_1) \\ m_2 \frac{d^2 b_2}{dt^2} &= -k_1(b_2 - b^*) - \frac{wd\rho Q^2}{2w^2} \left(\frac{1}{h^2} - \frac{1}{(h - b_2)^2} \right) + k_s(b_1 - b_2) \end{aligned} \quad (3.15)$$

where b^* is the resting position of both masses. The coupling term has been approximated as a linear term on the distances between each b . We will now make a change of variables, constructing the equivalent equation on h . This simplifies our problem, since closure at $h = 0$ is easily identifiable. We will impose the resting position to be $h_* = h$. Recall the definition $b_j + h_j = h$. The conversion yields

$$\begin{aligned} m_1 \frac{d^2 h_1}{dt^2} &= -k_1(h_1 - h) + \frac{wd\rho Q^2}{2w^2} \left(\frac{1}{h^2} - \frac{1}{h_1^2} \right) + k_s(h_2 - h_1) \\ m_2 \frac{d^2 h_2}{dt^2} &= -k_2(h_2 - h) + \frac{wd\rho Q^2}{2w^2} \left(\frac{1}{h^2} - \frac{1}{h_2^2} \right) + k_s(h_1 - h_2). \end{aligned} \quad (3.16)$$

We introduce the following parameters

$$\begin{aligned} h_1 &= h\tilde{h}_1, \quad h_2 = h\tilde{h}_2, \quad t = \sqrt{\frac{m_1}{k_1}}\tilde{t}, \\ \alpha &= \frac{m_2}{m_1}, \quad \lambda = \frac{k_2}{k_1}, \quad \omega = \frac{k_s}{k_1} \\ \beta &= \frac{wd\rho U_\infty^2}{2k_1 h} \end{aligned}$$

and the coupled fourth-order system of differential equations can be reduced to the nondimensional problem:

$$\begin{aligned} \frac{d^2 \tilde{h}_1}{d\tilde{t}^2} &= 1 - \tilde{h}_1 + \beta \left(1 - \frac{1}{\tilde{h}_1^2} \right) + \omega(\tilde{h}_2 - \tilde{h}_1) \\ \alpha \frac{d^2 \tilde{h}_2}{d\tilde{t}^2} &= \lambda(1 - \tilde{h}_2) + \beta \left(1 - \frac{1}{\tilde{h}_2^2} \right) + \omega(\tilde{h}_1 - \tilde{h}_2). \end{aligned} \quad (3.17)$$

The two mass model generalises the concepts from the original model we investigated, and maintains a lot of important features. Before investigating the behaviour of the coupled system of equations, we will verify that the new model can reproduce behaviours we have already seen. Namely, if we were to configure the problem as two equal masses with the same stiffness, and a strong coupling between them, then we would expect the oscillating behaviour of the original model to be replicated. We will then reduce the stiffness coupling and introduce different lateral stiffnesses for each mass, investigating how the oscillating components affect one another in a coupled system. Finally if we reduce the coupling to a negligible amount, we would then expect the masses to behave near independently.

For simplicity, we will from now on refer to the nondimensional dependent variables from Equation 3.17 as h_1 and h_2 , and the nondimensional time variable as t .

When examining individual cases, we often refer to the parameter quadruple $(\alpha, \lambda, \beta, \omega)$, instead of listing each parameter individually. For convenience, computations are always performed with initial conditions restricting the masses to rest, so the initial conditions (1, 2) mean the time-stepping MATLAB computation starts at $h_1 = 1, h_2 = 2$ with both at rest.

3.2 Behaviours of the two mass model

3.2.1 Strong coupling

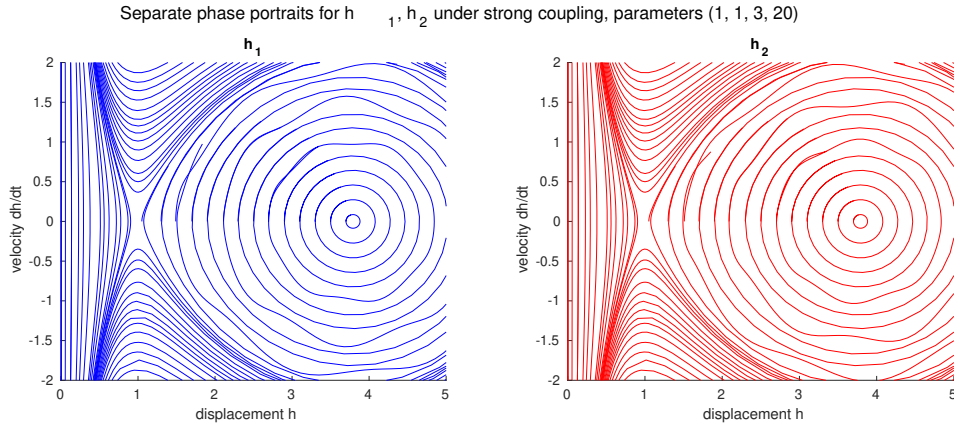


Figure 3.4: Separate phase portrait representations of solutions to the two mass model. Parameters (1, 1, 3, 20). High ω induces a strong coupling which replicates the behaviour of the single mass model. Perturbations of distance of between h_1 and h_2 of order 10^{-2} induce small oscillations, shown by the closed loops in the phase portraits which do not draw perfect circles.

We study the behaviour of two strongly coupled masses of equal stiffness, represented by $\alpha = 1, \lambda = 1, \omega \gg 1$. The coupled system of equations in Equation 3.17 take the same form for each. Similarly to the single-mass model, we can use the existence of stationary equilibria to determine the potential for oscillations to occur. Imposing the existence of a stationary equilibrium solution $h_1 = h_2 = x$ imposes that

$$1 - x + \beta \left(1 - \frac{1}{x^2}\right) = 0, \quad (3.18)$$

where the coupling term cancels. The stable equilibria exist at the positive zeroes of the function we define:

$$f(h) = 1 - h + \beta \left(1 - \frac{1}{h^2}\right). \quad (3.19)$$

Existence of zeroes is equivalent to the local maximum, belonging at $h = (2\beta)^{1/3}$ being positive-valued such that the zeroes exist, which can be written as

$$1 - (2\beta)^{\frac{1}{3}} + \beta \left(1 - (2\beta)^{\frac{-2}{3}}\right) \geq 0, \quad (3.20)$$

with equality if there is only one equilibrium solution. Equation 3.20 reduces to

$$\frac{(1 + \beta)^3}{\beta} \geq \frac{27}{4}. \quad (3.21)$$

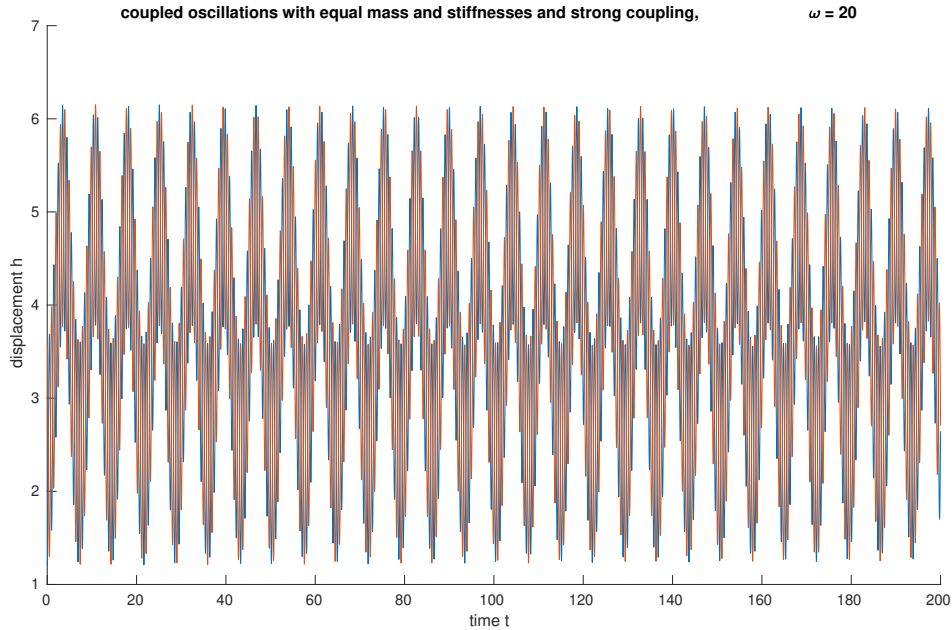


Figure 3.5: Coupled oscillations under parameters $(1, 1, 3, 20)$ and initial conditions $h_1 = 1.2, h_2 = 3.59$. The pair of masses, forced into different initial positions, oscillate about each other rapidly, while following a dominant oscillation path.

We will reiterate that this is the condition specifically for $\lambda = 1$. When this is the case, this equation is satisfied for all positive $\beta > 0$ and has equality at $\beta = 0.5$. If the initial conditions for h_1, h_2 set their individual positions between the two equilibrium solutions, provided they exist, then we observe coupled oscillations as in Figure 3.5. The equilibria, being the solutions of Equation 3.19, are identical for both components of the system of differential equations, provided the parameters satisfy $\alpha = 1, \lambda = 1, \omega \gg 1$ in order to model two strongly coupled masses. This allows us to discuss the solutions to a single equation without loss of generality. Assuming there exist equilibria x , we can construct the Jacobian and determine the stability local to these equilibria. We regard the whole system with the variable $h_1 = h_2 = h$. The system of derivatives in the single case can be written as

$$\begin{aligned} \frac{dh}{dt} &= g \\ \frac{dg}{dt} &= f(h) = 1 - h + \beta \left(1 - \frac{1}{h^2}\right), \end{aligned} \quad (3.22)$$

which vectorises as

$$\frac{d}{dt} \begin{pmatrix} h \\ g \end{pmatrix} = \begin{pmatrix} g \\ f(h) \end{pmatrix}. \quad (3.23)$$

Recall we have stationary equilibria which we call x . We compute the Taylor series of $f(h)$ local to

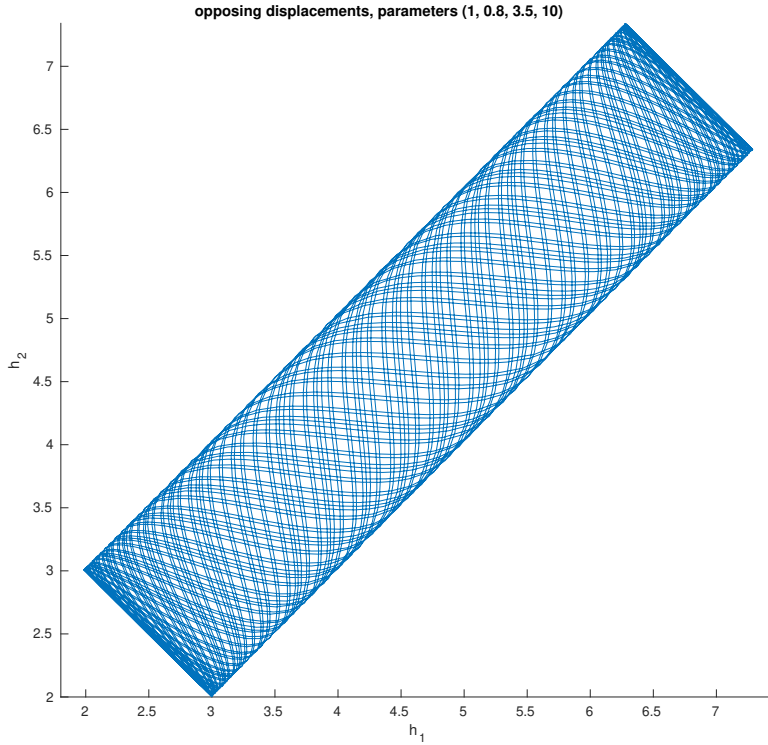


Figure 3.6: Plot of opposing displacements (h_2 against h_1). The motion is constrained within a fixed region, however it is quasiperiodic since the oscillations will, given infinite time, fill the entire illustrated area. Important parameters are $\omega = 10$, $\lambda = 0.8$ so the stiffnesses are not equal and the masses are strongly constrained together.

this point.

$$f(h) = f(x) + (h-x)f'(x) + (h-x)^2 \frac{f''(x)}{2!} + \dots = \sum_0^{\infty} (h-x)^n \frac{f^{(n)}(x)}{n!}. \quad (3.24)$$

Similarly to our earlier reasoning, we truncate the Taylor series to the first order approximation $f(h) \approx (h-x)f'(x)$, where the constant term disappears. The vectorised approximation becomes

$$\frac{d}{dt} \begin{pmatrix} h \\ g \end{pmatrix} = \begin{pmatrix} g \\ (h-x)f'(x) \end{pmatrix}. \quad (3.25)$$

Substituting $U = h - x$ and $V = g$ we obtain

$$\frac{d}{dt} \begin{pmatrix} U \\ V \end{pmatrix} = \begin{bmatrix} 0 & 1 \\ f'(x) & 0 \end{bmatrix} \begin{pmatrix} U \\ V \end{pmatrix} \quad (3.26)$$

We can inspect the eigenvalues of this matrix to determine the stability of the equilibrium solutions. Having studied the single mass model, we would expect the potential for any of zero, one or two

equilibrium solutions, with oscillations occurring in the case of two individual stationary points. However, the model differs from the single mass model by the feature that there always exists at least one equilibrium solution. This is because the solution $(1, 1)$ always satisfies the differential equations. In the section on intermediate coupling, and from then on, we will derive stronger results on existence of equilibrium solutions.

Forcing a strong coupling replicates the behaviour of the single mass model, as shown in Figure 3.4. We have closed orbits around a stationary point, and diverging trajectories close to an unstable point. For additional insight, we have forced minor perturbations of distance between h_1 and h_2 at the initial conditions, and we observe small oscillations in the trajectories. If these paths belong to the family of closed orbits, then the oscillations between each other may continue for an extended period of time.

3.2.2 Intermediate coupling force, equilibria

We now develop our analysis of the two mass model by examining multiple dimensions of the parameter space. First, we will retain the stiffness coupling $\omega \gg 1$, but consider the cases induced by $\lambda \neq 1$, which are where the relative stiffnesses for each component are not the same. We freely change β since it is similar to a forcing term, which we can change to observe different behaviours of the model.

In general, we observe quasiperiodic oscillating motion of the masses. We will clarify the behaviours that we would expect the coupled system to exhibit. Firstly, the masses may oscillate indefinitely within a bounded region. A trivial subclass of this behaviour would be the masses resting in a stationary equilibrium. Alternatively, we could experience closure, with or without oscillations beforehand.

Figure 3.6 demonstrates indefinite oscillations under a high coupling force. The borders of the shape accommodate the restrictions of the coupling force and the individual stiffness of the masses.

We would expect the equilibria instead to be the solutions of two equations for each component, being:

$$\begin{aligned}\hat{f}_1(h) &= 1 - h + \beta \left(1 - \frac{1}{h^2}\right) &= 0 \\ \hat{f}_2(h) &= \lambda(1 - h) + \beta \left(1 - \frac{1}{h^2}\right) &= 0.\end{aligned}\tag{3.27}$$

We have neglected the α term in this case since it is a scaling of the second equation and is never 0, so a zero of \hat{f}_2 satisfies our needs regardless of the value of α . The local maximum of \hat{f}_1 is at $h = (2\beta)^{1/3}$, and for \hat{f}_2 the local maximum is $h = (2\beta/\lambda)^{1/3}$. Hence, the existence of equilibrium solutions is expected to be determined by two assumptions, being

$$\begin{aligned}\hat{f}_1\left((2\beta)^{\frac{1}{3}}\right) &\geq 0, \\ \hat{f}_2\left(\left(\frac{2\beta}{\lambda}\right)^{\frac{1}{3}}\right) &\geq 0,\end{aligned}$$

where if both are satisfied, then each mass has one or two points in space where it belongs to a state of stationary equilibrium. It is not immediately clear, but this equation is actually always satisfied with at least equality. However, note the assumption that $h_1 = h_2$ which we made when exploring earlier cases, which is no longer a valid assumption to make. Therefore, we cannot neglect the stiffness coupling term, which makes it much harder to determine potential points of equilibrium of the system. We will refer to the solutions of Equation 3.27 as the *particular equilibria*, while

the actual solutions to the coupled equations will be referred to as the *general equilibria*. If we are to define the properties of stationary equilibria more rigorously, we will be able to understand the properties of the model better. We want all equilibrium solutions $h_1 = x, h_2 = y$ which solve the

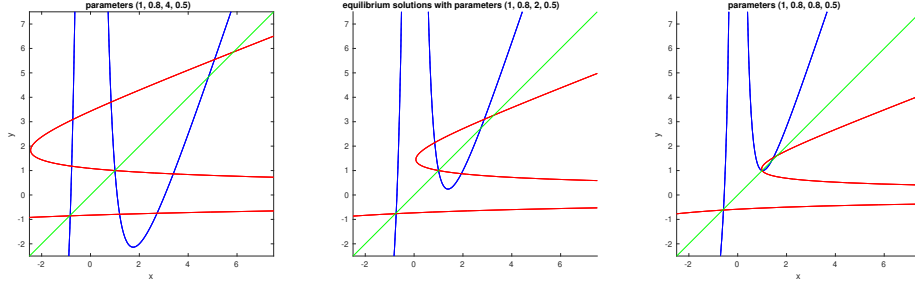


Figure 3.7: Curves A (left), B (middle), C (right), representing the equilibrium solutions to the coupled equations under separate parameters. The x and y axes are the equilibrium solutions of $f_1 = 0$ and $f_2 = 0$ respectively. In all graphs, the blue curve is the family of all equilibrium solutions for x , the red curve is the family of solutions for y , and the green line is the line $y = x$. Curves A, B and C all feature parameters $\alpha = 1$, $\lambda = 0.8$, $\omega = 0.5$, changing β , where $\beta_A = 4$, $\beta_B = 2$, $\beta_C = 0.8$. The red and blue curves intersect at points $f_1 = f_2 = 0$, which are equilibrium solutions satisfying both equations. The points at which a curve intersects the $y = x$ line are the points that satisfy equilibrium of that equation, and also satisfy $y = x$, which cancels the coupling term. These are the solutions of $\hat{f}_1 = \hat{f}_2 = 0$ which we covered earlier. Negative solutions do exist but must be ignored since we cannot accommodate negative values for h_1, h_2 in the model.

coupled differential equations. From here on, an equilibrium solution is a pair $(h_1, h_2) = (x, y)$. We make the definition

$$\begin{aligned} f_1(x, y) &= 1 - x + \beta \left(1 - \frac{1}{x^2} \right) + \omega(y - x) \\ f_2(x, y) &= \lambda(1 - y) + \beta \left(1 - \frac{1}{y^2} \right) + \omega(x - y). \end{aligned} \quad (3.28)$$

Then the system we are solving can be written as

$$\begin{aligned} \frac{d^2x}{dt^2} &= f_1(x, y) \\ \alpha \frac{d^2y}{dt^2} &= f_2(x, y) \end{aligned} \quad (3.29)$$

and we want to solve for equilibrium solutions. It suffices to solve $f_1(x, y) = f_2(x, y) = 0$ to generate equilibrium solutions, since α only changes the equation up to scaling. An equilibrium solution is now a pair (x, y) which solve both equations, thus the problem can be reduced to

$$1 - x + \beta \left(1 - \frac{1}{x^2} \right) + \omega(y - x) = \lambda(1 - y) + \beta \left(1 - \frac{1}{y^2} \right) + \omega(x - y) = 0. \quad (3.30)$$

Our solutions are determined by two non-linear homogeneous equations involving three parameters (λ, β, ω) , which we want to solve for two variables (x, y) . This is a challenge to solve, but to start we know from the formulation of the model and the nondimensionalisation that $(x, y) = (1, 1)$ is

an equilibrium solution for all values of the parameters. Solutions are found by computation via Newton's method. Figure 3.7 visualises the families of solutions to the equations. The iterative method starts by using Newton's method to solve the separated equations, neglecting the stiffness coupling. These individual stationary points are used as starting positions for implementation of the MATLAB `fsolve()` function, solving the homogeneous equation $F = [f_1(x, y), f_2(x, y)]^T = \mathbf{0}$, to find a true equilibrium solution (x, y) . In most cases, there are four individual equilibrium solution pairs to the coupled equations, being the strictly positive intersection points of the hyperbolas in Figure 3.7. The negative regions are included in the figure for visualisation of the shape of the curves, but the negative-valued solutions are invalid forms of equilibrium for our formulation of the problem. We will refer to the solution pairs close to the line $y = x$ as the *diagonal equilibria*, and the other solutions as the *off-diagonal equilibria*. On inspection, as the extrema of the curves approach each other, the off-diagonal equilibria converge and annihilate.

Solutions to Equation 3.30 can fortunately be computed to any accuracy we require, however an important question involves the existence of solutions themselves. We want to know, depending on the parameters, how many solutions exist. The equations themselves can be arranged into the couple,

$$\begin{aligned}(\omega + \lambda)y^3 - (\lambda + \beta)y^2 - \omega xy^2 + \beta &= 0 \\(1 + \lambda)x^3 - (1 + \beta)x^2 - \omega yx^2 + \beta &= 0.\end{aligned}\tag{3.31}$$

where each equation is linear in one variable and polynomial (a nicer form of non-linear) in the other. Rearrange the equation linear in x to write it in terms of y and then substitute back to obtain

$$(1 + \omega) \left(\left(1 + \frac{\lambda}{\omega} y \right) + \frac{\beta}{\omega y^2} - \frac{\lambda + \beta}{\omega} \right)^3 - (1 + \beta + \omega y) \left(\left(1 + \frac{\lambda}{\omega} y \right) + \frac{\beta}{\omega y^2} - \frac{\lambda + \beta}{\omega} \right)^2 + \beta = 0.\tag{3.32}$$

However we have to keep in mind the requirements on the variables. We must have that all parameters λ , β , ω are strictly positive, and likewise for x and y . Since we have eliminated x , we have actually gained solutions, since it is possible for a solution to exist for a positive y and negative x , which is a solution for this equation. We require the polynomial term to be strictly positive as a qualification for solutions.

We want to evaluate the stability of the equilibrium solutions for the two mass model. We first truncate the Taylor series of f_1 and f_2 about an equilibrium point (x_0, y_0) to the first order approximation, yielding the equations

$$\begin{aligned}\frac{d^2x}{dt^2} &= f_1(x_0, y_0) + \left(\frac{\partial f_1}{\partial x}(x_0, y_0) \right) (x - x_0) + \left(\frac{\partial f_1}{\partial y}(x_0, y_0) \right) (y - y_0) \\ \alpha \frac{d^2y}{dt^2} &= f_2(x_0, y_0) + \left(\frac{\partial f_2}{\partial x}(x_0, y_0) \right) (x - x_0) + \left(\frac{\partial f_2}{\partial y}(x_0, y_0) \right) (y - y_0).\end{aligned}\tag{3.33}$$

The constant terms vanish by the definition of the equilibrium solutions. Introduce $u = x - x_0$ and $v = y - y_0$. Since u and x are linear in each other, there is no complication in changing between variables for the governing equations. The same applies with v and y . The system becomes

$$\begin{aligned}\frac{d^2u}{dt^2} &= \left(\frac{\partial f_1}{\partial x}(x_0, y_0) \right) u + \left(\frac{\partial f_1}{\partial y}(x_0, y_0) \right) v \\ \frac{d^2v}{dt^2} &= \frac{1}{\alpha} \left(\frac{\partial f_2}{\partial x}(x_0, y_0) \right) u + \frac{1}{\alpha} \left(\frac{\partial f_2}{\partial y}(x_0, y_0) \right) v.\end{aligned}\tag{3.34}$$

Now introduce the variables \hat{u} , \hat{v} such that $du/dt = \hat{u}$ and $dv/dt = \hat{v}$. This formulates the linear system:

$$\begin{aligned}\frac{du}{dt} &= \hat{u} \\ \frac{d\hat{u}}{dt} &= \left(\frac{\partial f_1}{\partial x}(x_0, y_0) \right) u + \left(\frac{\partial f_1}{\partial y}(x_0, y_0) \right) v \\ \frac{dv}{dt} &= \hat{v} \\ \frac{d\hat{v}}{dt} &= \frac{1}{\alpha} \left(\frac{\partial f_2}{\partial x}(x_0, y_0) \right) u + \frac{1}{\alpha} \left(\frac{\partial f_2}{\partial y}(x_0, y_0) \right) v.\end{aligned}\tag{3.35}$$

We have obtained the Jacobian for the system, appearing in the matrix equation:

$$\frac{d}{dt} \begin{pmatrix} u \\ \hat{u} \\ v \\ \hat{v} \end{pmatrix} = \begin{bmatrix} 0 & 1 & 0 & 0 \\ \frac{\partial f_1}{\partial x}(x_0, y_0) & 0 & \frac{\partial f_1}{\partial y}(x_0, y_0) & 0 \\ 0 & 0 & 0 & 1 \\ \frac{1}{\alpha} \frac{\partial f_2}{\partial x}(x_0, y_0) & 0 & \frac{1}{\alpha} \frac{\partial f_2}{\partial y}(x_0, y_0) & 0 \end{bmatrix} \begin{pmatrix} u \\ \hat{u} \\ v \\ \hat{v} \end{pmatrix}.\tag{3.36}$$

In prior examples, the problems have involved second order systems, whereas our current problem is fourth order, hence the 4×4 matrix \mathbf{J} . The definitions of these partial derivatives are as follows:

$$\begin{aligned}\frac{\partial f_1}{\partial x}(x, y) &= -1 + 2\beta x^{-3} - \omega \\ \frac{\partial f_1}{\partial y}(x, y) &= \omega \\ \frac{\partial f_1}{\partial x}(x, y) &= \omega \\ \frac{\partial f_2}{\partial y}(x, y) &= -\lambda + 2\beta y^{-3} - \omega\end{aligned}\tag{3.37}$$

We will later refer to these definitions of the partial derivatives in order to analyse the matrix \mathbf{J} and its properties. Eigenvalues of \mathbf{J} are the constant terms σ which satisfy the equation $\mathbf{J} - \sigma\mathbf{I} = \mathbf{0}$. Including zero, μ always has four values for any form of \mathbf{J} . At an equilibrium point (x_0, y_0) , the eigenvalues σ of the Jacobian are given explicitly by the characteristic polynomial

$$\sigma^4 + \left(\frac{\partial f_1}{\partial x}(x_0, y_0) \right) \sigma^2 + \left(\frac{\partial f_1}{\partial x}(x_0, y_0) \frac{\partial f_2}{\partial y}(x_0, y_0) - \omega^2 \right) = 0.\tag{3.38}$$

3.2.3 Oscillations and closure

We provide results to explore the stability of equilibria by computing and examining behaviours, and explore interesting behaviours that occur as a result. Figure 3.8 highlights equilibrium solutions and the consequence of finite precision arithmetic. In Figure 3.9, by reversing the initial conditions of the objects, the results are indicative of the behaviours in which oscillations occur.

The general behaviour of the model is for the two masses to move indefinitely in a quasiperiodic orbit about an equilibrium solution. The motions of the masses are bounded and exhibit clear oscillations, hence on a long time scale we can identify motion that appears periodic and stable. However on a small timescale we observe irregularity. Irregular behaviour may or may not be periodic in nature and we cannot determine this easily. If we observe a pattern in the data plot, we

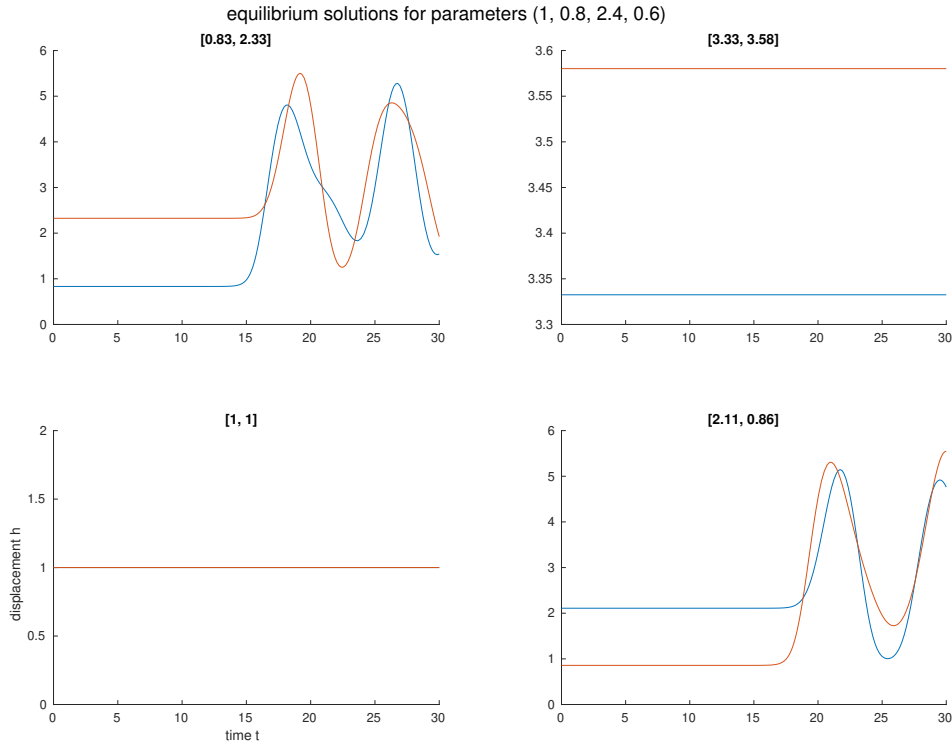


Figure 3.8: Computation of behaviours starting at equilibrium solutions. Parameters $\alpha = 1$, $\lambda = 0.8$, $\beta = 2.4$, $\omega = 0.6$. Initial conditions title each subfigure. We use the MATLAB `fsolve()` command to find the equilibrium solutions, and the finite precision arithmetic is unable to store their values exactly. As such, the paths eventually diverge from equilibrium in the unstable cases.

want to know if these behaviours eventually repeat themselves (periodic) or if there is an irrational relationship between the oscillating masses and small scale irregular behaviour is never repeated, despite appearing periodic on a large time scale (quasiperiodic). Even if we can determine the nature of this, it may be difficult to determine whether the determined behaviour is actually in the nature of the model, or if the finite-precision numerical computation of the model introduces irregularity.

In particular, we often observe behaviour in the plot of displacement against time which is apparently quasiperiodic, where small scale irregular motions do not repeat themselves. Quasiperiodic motion occurs in both the scale where it is an evident feature of the model, and also on the smaller scale where it is difficult to distinguish from numerical error introducing an irregularity to the computation.

It is difficult to determine whether or not we will observe closure in a computation, judging only by initial conditions and observed features of the model. Analytically, the expression for acceleration in the system of ODEs diverges to $-\infty$ as either $h_1 \rightarrow 0$ or $h_2 \rightarrow 0$, due to the $1/h^2$ terms in both ODEs. In order for closure to occur, one of the masses must be perturbed enough towards zero that the system loses stability and collapses. There is often a bound for oscillations, within which the quasiperiodic orbits will continue indefinitely.

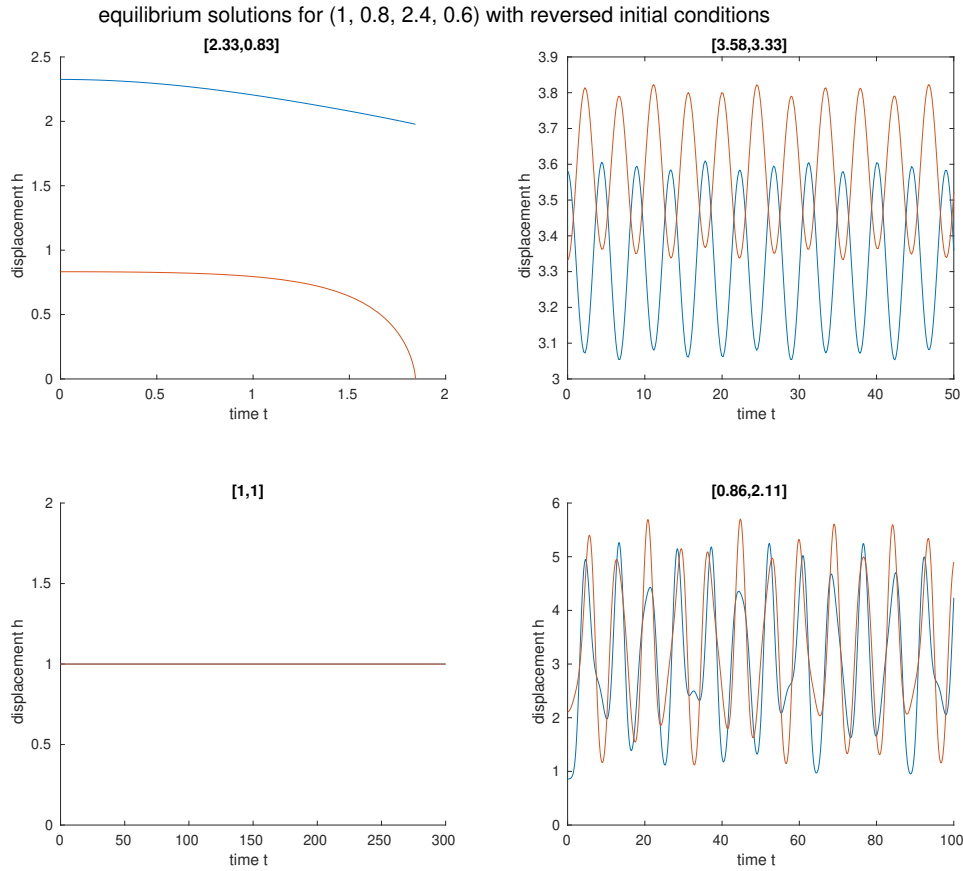


Figure 3.9: Reversing the initial conditions of Figure 3.8. The right-most subfigures are of most interest. In the case of initial conditions (3.58, 3.33) we have oscillations that appear regular, but in the initial conditions (0.86, 2.11) the behaviours are much more irregular. The purpose of this figure is to show that equilibrium solutions are rarely symmetric, and reversing the initial conditions leads to fundamentally different results.

3.3 A collection of results

In general, equilibrium solutions are not affected by the mass quotient α , so in most cases $\alpha = 1$ for simplicity. For readability, numerical values will be given to two decimal places.

3.3.1 Four stationary points

Consider the parameter configuration (1, 0.8, 3, 0.3), where we have a difference in stiffness and a smaller stiffness coupling. There are four equilibrium solutions. The diagonal equilibria are (1, 1) and (3.94, 4.39), and the off-diagonal equilibria are (0.88, 3.47) and (3.03, 0.90). With the Jacobian as in

Eigenvalues of equilibrium solutions, mapped in the complex plane, in the case of parameters (1, 0.8, 3, 0.3)

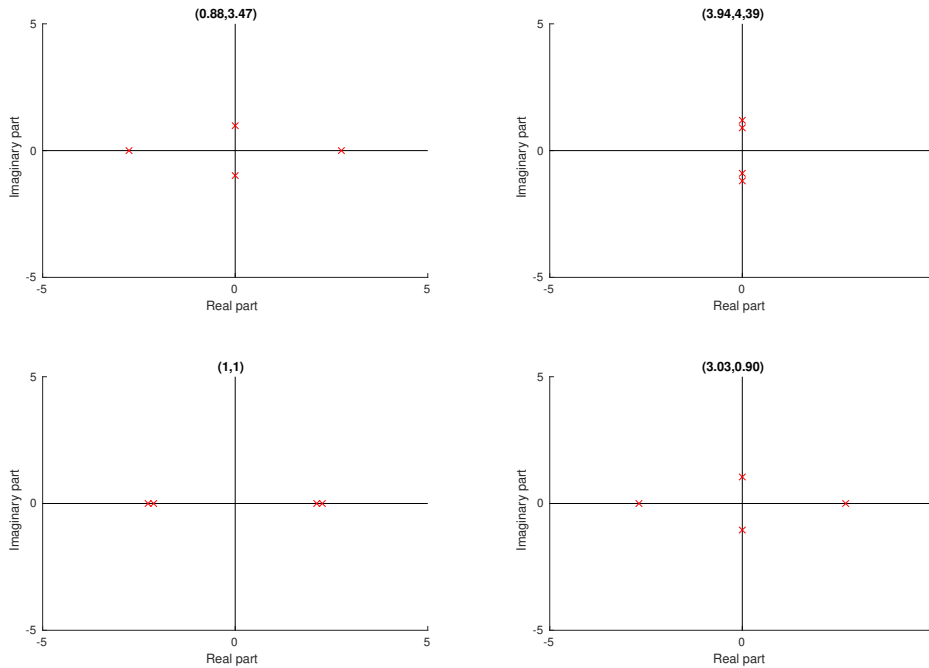


Figure 3.10: Plots in the complex plane of the eigenvalues of equilibrium solutions, in a particular case where four such solutions exist. The diagonal solutions provide eigenvalues that are either entirely real or entirely imaginary, while the off-diagonal solutions provide pairs of real and imaginary eigenvalues.

Equation 3.36, the diagonal solution (1, 1) has entirely real eigenvalues, and (3.94, 4.39) has entirely imaginary eigenvalues. Each off-diagonal solution has a combination, with one pair of eigenvalues being entirely imaginary and the other being entirely real. See Figure 3.10 for a visualisation of the eigenvalues for the steady solutions in this example. We can see that all equilibrium solutions, except for (3.94, 4, 39), bear an eigenvalue with positive real part, and are thus unstable.

The existence of four equilibrium solutions is the most common case we observe with the model. Continuous orbits may occur which run indefinitely, with small scale quasiperiodic behaviour, similar to the behaviour shown in Figure 3.13.

See Figures 3.11 and 3.12. In the former, the shape of the curve indicates quasiperiodic orbits. The behaviour of the curve is almost periodic, since the path taken in this representation are regularly repeated up to a small difference. The latter shows time series and phase portrait representations of another behaviour in this parameter configuration. We can identify quasiperiodicity from the visibly repeating pattern in the time series, and the clearly outlined distinct orbit cycles in the phase portrait.

The model often exhibits continuous coupled quasiperiodic orbits. Under the motivation of understanding voiced sounds from a mathematical model, we can claim that this resembles the complex structure of the tones produced from the vocal folds.

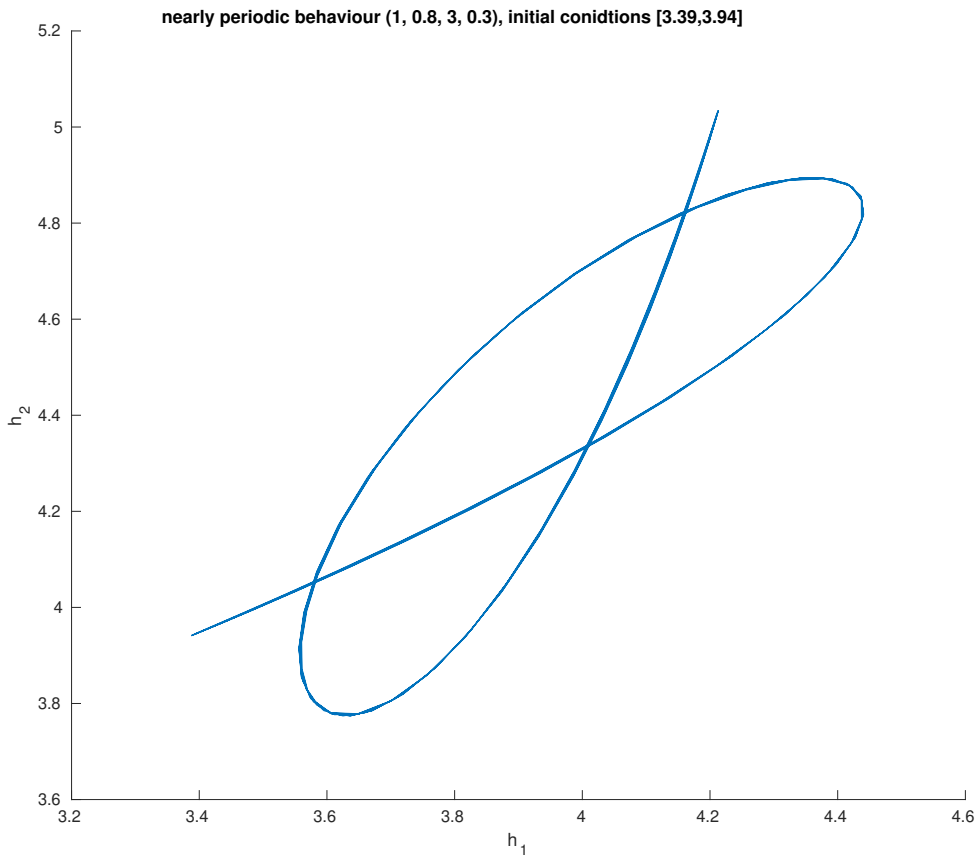


Figure 3.11: Distance plot of h_2 against h_1 for $t = 100$. In the parameter configuration $(1, 0.8, 3, 0.3)$, with initial positions $(3.39, 3.94)$, it is possible to obtain results that very closely resemble periodic orbits. Over long time span computations with low tolerance, the orbit may diverge from the curve shown and eventually fill a bounding rectangle. Later on, we will provide analysis of the reliability of results.

3.3.2 Converged stationary points and fundamentally different solutions

In the case where the parameters take the values $(1, 0.3, 1, 0.8)$, then we have exactly two equilibrium solutions, being $(1, 1)$ and $(2.15, 2.62)$. The solution $(2.15, 2.62)$ is stable, with eigenvalues $\pm 1.47i$ and $\pm 0.67i$ all being entirely imaginary. However the solution $(1, 1)$ has eigenvalues ± 1.19 and $\pm 0.57i$, with one eigenvalue with positive real part. The case of exactly two equilibrium solutions does not yield fundamentally different results from when four are present. See Figure 3.8 and look at the particular cases of the off-diagonal equilibria, which disappear in the case of two stationary points. In the case shown, these equilibria are so unstable that machine precision struggles to maintain their stationary nature and they soon diverge. Since the off-diagonal equilibria converge onto the solution $(1, 1)$, the affect of any unstable equilibria on the problem is entirely on this single

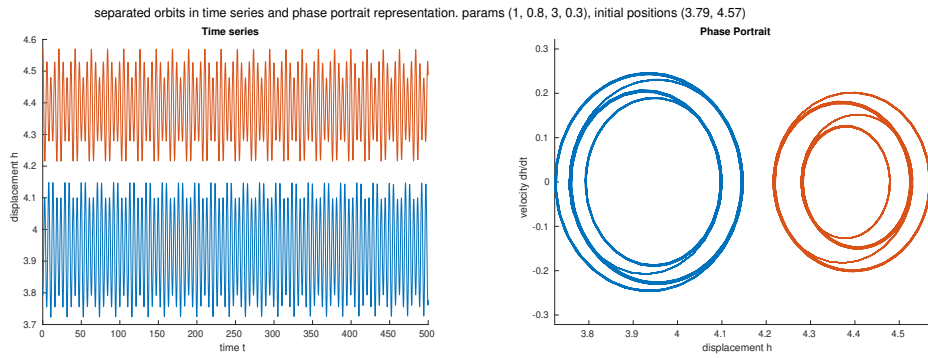


Figure 3.12: Time series and phase portrait representation of a clearly quasiperiodic pattern. Computed under parameters $(1, 0.8, 3, 0.3)$ with initial positions $(3.79, 4.57)$. Orbits are represented in the phase portrait by distinct closed loops, and the pattern of oscillations always moves between loops in a consistent pattern. The orbits are bounded and their regions of distance are disjoint.

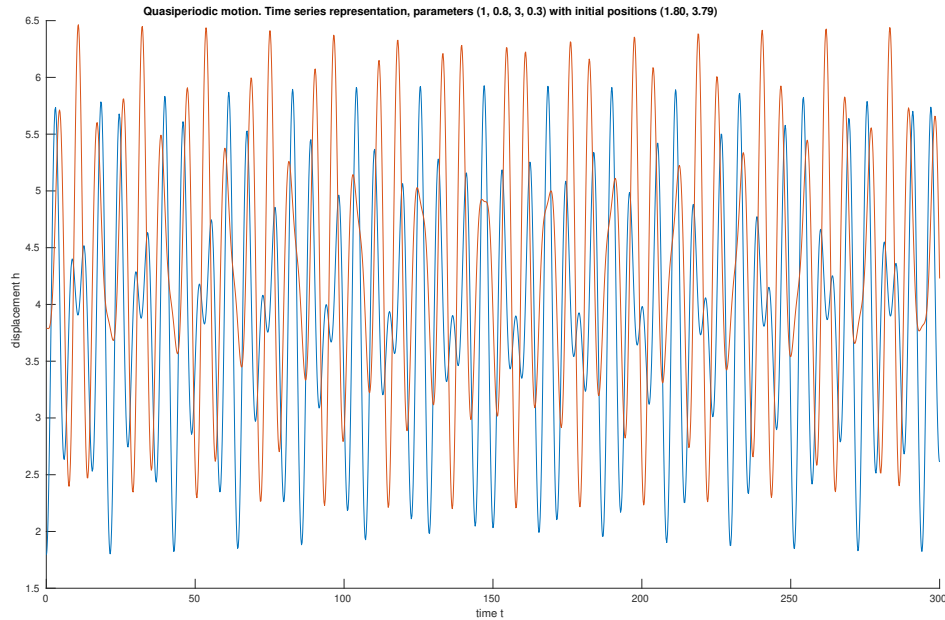


Figure 3.13: Time series of h_1 (blue) and h_2 (orange). Computed with parameters $(1, 0.8, 3, 0.3)$ with initial positions $(1.80, 3.79)$. Quasiperiodic motion, with regular shape of oscillation orbit, but irregular motion.

point. The appearance of the diagonal equilibria in Figure 3.10 are similar to this case.

In the case of exactly one equilibrium solution, we can say with certainty that it is the solution $(1, 1)$, which is always a solution to the model under all parameters. The consistent single equilibrium

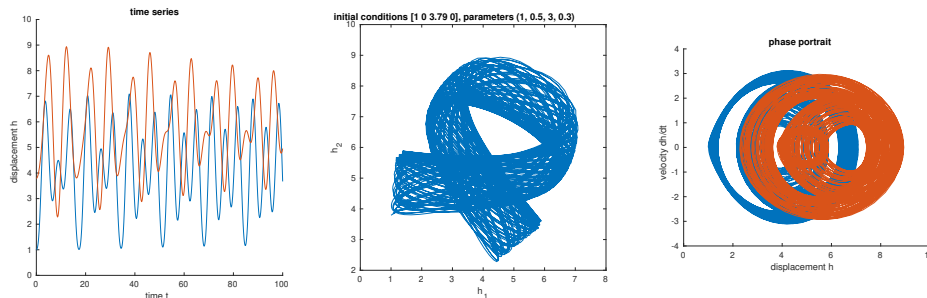


Figure 3.14: An interesting result in time series, opposing displacement and phase portrait representation. We set parameters $(1, 0.5, 3, 0.3)$ and initial conditions on the plates $(1, 3.79)$. We observe a nested pattern of orbits, where there are three distinct circles in the phase portrait for each mass and we move between orbits in a regular pattern.

solution $(1, 1)$ has a unique property, in which it is the only equilibrium solution of the model where the stiffness coupling terms always cancel. In cases with more than one solution, the other diagonal equilibrium solution may be a solution (x, x) for $x \neq 1$, but this is not guaranteed. The conditions for oscillations, which we explored in Equation 3.27, give us the conditions $\beta = 0.5$, $\lambda = 1$ to guarantee the existence of exactly one equilibrium solution. The value of ω is unrestrained, since the stiffness term itself is cancelled by the solution at $(1, 1)$ being the only solution to the equations.

Consider the configuration of parameters $(1, 1, 0.5, 2)$, which guarantees the existence of the single equilibrium solution $(1, 1)$. Results show that the eigenvalues of the Jacobian matrix are the complex conjugate pair $0 \pm 2i$ and the repeated solution 0 . The zero eigenvalue is unique to particular choices of the parameters. Note the partial derivatives used in the Jacobian, for which the definitions are given in Equation 3.37. If $\beta = 0.5$ and $\lambda = 1$, then at $(x, y) = (1, 1)$, the Jacobian from Equation 3.36 becomes

$$\mathbf{J} = \begin{bmatrix} 0 & 1 & 0 & 0 \\ -\omega & 0 & -\omega & 0 \\ 0 & 0 & 0 & 1 \\ \omega & 0 & \omega & 0 \end{bmatrix},$$

and this is not a full rank matrix, hence the zero eigenvalues.

3.3.3 Unique behaviours

We can generate a particular case under parameters $(1, 0.5, 3, 0.3)$ which produces extremely interesting images. Figure 3.14 shows multiple representations of a computation, where the phase portrait shows nested cycles. Each plate h_1 , h_2 has three orbits in the phase portrait of distinct radius. However, the regularity in which each plate passes into each orbit is consistent, as shown by the opposing displacement plot. The opposing displacement plot itself is of high interest since it draws a bounded region of the orbits.

We will explore extended behaviours of this example, as well as others, later on when discussing verification of energy. For now, briefly see Figure 3.16. The two plates oscillate around the equilibrium solution $(4.31, 5.88)$. In this case, the eigenvalues of this equilibrium can be computed at $\pm 1.17i$ and $\pm 0.79i$, which are purely imaginary. This case is similar to the eigenvalues of equilibria represented in Figure 3.10. All eigenvalues belong to the same regions of the complex p

3.4 Verification of results

Numerical methods do not provide exact results and it is very easy to produce results which seem plausible but are fundamentally wrong. We will introduce a few concepts that will allow us to verify solutions. Most results from the two mass model will be unreliable if the tolerances are not strict enough. See the appendix for a review on unstable results.

3.4.1 Numerical methods

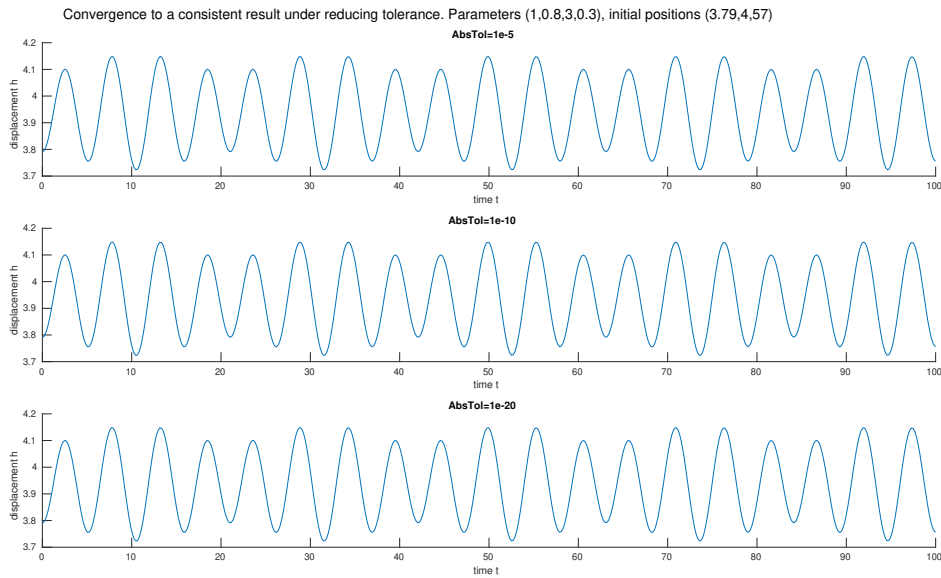


Figure 3.15: Results converging to a consistent solution. Under stepping down the tolerance AbsTol from 10^{-5} to 10^{-20} , we maintain consistent results in this case. Computed under parameters (1, 0.8, 3, 0.3) with initial positions (3.79, 4.57) visualising displacement of h_1 only. In MATLAB, the tolerance AbsTol can be set arbitrarily, however extremely small tolerances are infeasible and fail to provide any solution at all.

One concern in computation is the existence of numerical error. It is possible that the discretisation could induce a local error to the numerical solution and this small difference could lead to a divergence in the result.

The ordinary differential equation solvers in MATLAB feature options which can be modified using the `odeset` struct. We are particularly interested in the parameters AbsTol and RelTol , which affect the precision of the numerical solution [7]. The value for AbsTol gives a lower bound on the magnitude of the solution, encouraging the timestepping algorithm to remain above a particular magnitude. If the solution approaches zero asymptotically, this will reach a point where the solver fails. The RelTol term instead controls a termwise precision of the solution, comparing a term in the timestep to an immediately previous solution. If we decrease RelTol , the numerical values will be closer to the exact solution for our initial conditions.

The differential equation solvers in MATLAB implement Runge-Kutta methods of different order [8]. For example, `ode45()` applies one method where the error is order $\mathcal{O}(h^4)$ and another with error of order $\mathcal{O}(h^5)$, where h is the length of a time step. If we wish, we can implement a different solver such as `ode89`, which uses methods of eighth and ninth order error. These solvers are extremely accurate when the time steps are sufficiently small, however they are also extremely computationally expensive. The sufficient method for computations in our case is to use `ode45`, where we step down `AbsTol` and `RelTol` as required. In MATLAB, error is estimated by the difference in magnitude between two numerical solutions, which is assumed to be greater than the error from one method to the exact solution.

3.4.2 Energy of the system

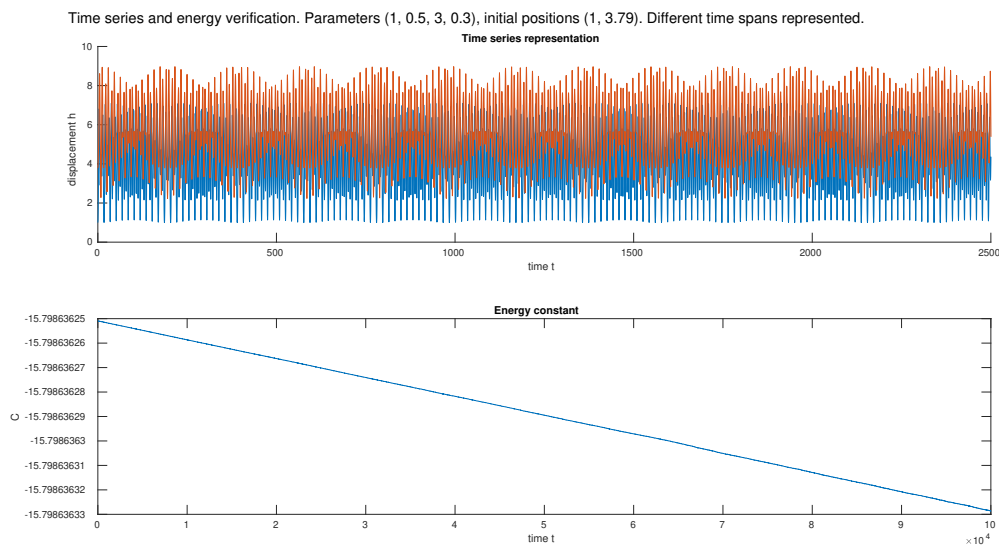


Figure 3.16: Attempting to verify the result of nested orbits we have seen in Figure 3.14. The upper plot shows the same time series truncated at $t = 3000$. The lower plot uses the energy constant defined in Equation 3.39. The energy constant accrues miniscule error from the initial conditions over the time span of the computation.

We can also find a method of verification which relates to the energy of the system. Recall the equations of motion which are given by Equation 3.17. We want to rearrange these equations and integrate, similar to what we did in the previous section, in order to find an expression that resembles the kinetic energy of the system. First, we will write $u = h_1$, $v = h_2$ for convenience, and express the equations of motion in the form

$$\begin{aligned}\frac{d^2u}{dt^2} &= 1 - u + \beta \left(1 - \frac{1}{u^2}\right) + \omega(v - u) \\ \alpha \frac{d^2v}{dt^2} &= \lambda(1 - v) + \beta \left(1 - \frac{1}{v^2}\right) + \omega(u - v).\end{aligned}$$

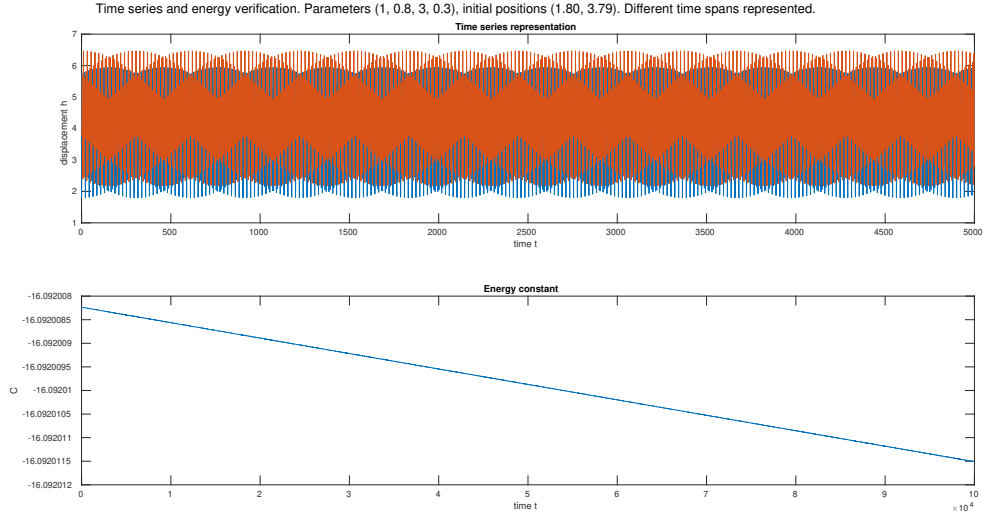


Figure 3.17: Second verification via energy constant. Parameters (1, 0.8, 3, 0.3) with initial positions (1.80, 3.79). The computation still diverges over time, although energy is lost very slowly. Under a strong enough tolerance, results can be reliable for very long time spans.

Define functions \hat{f} and \hat{g} as follows

$$\hat{f}(u) = 1 - u + \beta \left(1 - \frac{1}{u^2} \right)$$

$$\hat{g}(v) = \lambda(1 - v) + \beta \left(1 - \frac{1}{v^2} \right).$$

Now define functions F and G

$$F(u) = u - \frac{1}{2}u^2 + \beta \left(u - \frac{1}{u} \right)$$

$$G(v) = \lambda \left(v - \frac{1}{2}v^2 \right) + \beta \left(v - \frac{1}{v} \right).$$

These functions satisfy $dF/du = \hat{f}(u)$ and $dG/dv = \hat{g}(v)$. We can write the system of differential equations in the form

$$\frac{d^2u}{dt^2} = \hat{f}(u) + \omega(v - u)$$

$$\alpha \frac{d^2v}{dt^2} = \hat{g}(v) + \omega(u - v).$$

We will perform a rearranging of the expression on the second derivative of u , but we will not go into detail on the derivation for the second expression, since it is virtually identical. First, we multiply the whole equation by the first derivative of u with respect to t ,

$$\frac{du}{dt} \frac{d^2u}{dt^2} = \frac{du}{dt} \hat{f}(u) + \omega \frac{du}{dt} (v - u).$$

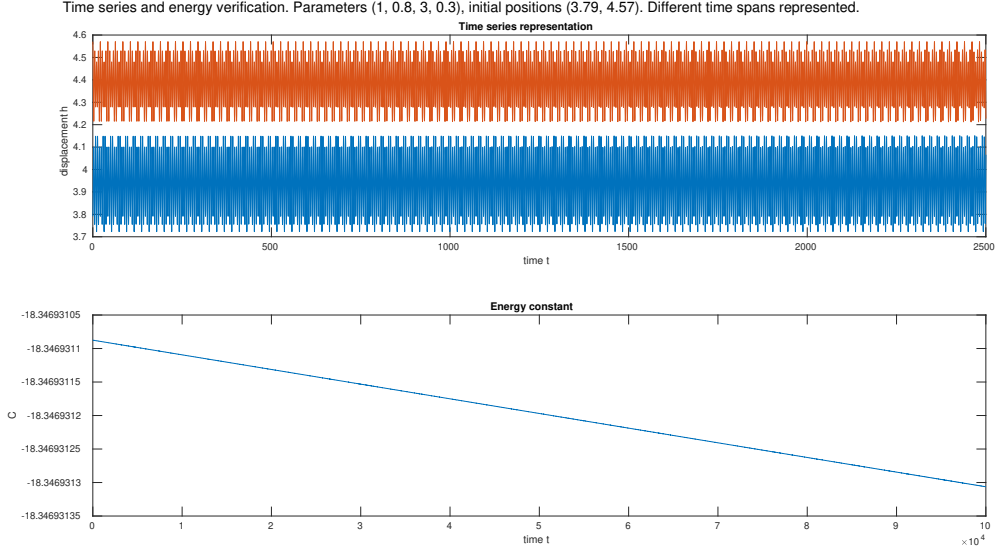


Figure 3.18: Third verification via energy constant. Parameters (1, 0.8, 3, 0.3) with initial positions (3.79, 4.57). Regular orbits in disjoint bounds. Under particular initial conditions, parameters, and time span, the system maintains a regular behaviour for which the energy constant is approximately maintained. See that the value of the energy constant does not change up to the first two decimal places. We have restricted the time span of the computation to force that the solution is more reliable than other results.

This expression can be written mostly as derivatives, equivalently,

$$\frac{d}{dt} \left(\frac{1}{2} \left(\frac{du}{dt} \right)^2 \right) = \frac{d}{dt} F(u) - \omega \frac{d}{dt} \left(\frac{1}{2} u^2 \right) + \omega v \frac{du}{dt}.$$

Applying the same method to the second equation, we obtain

$$\frac{d}{dt} \left(\frac{1}{2} \alpha \left(\frac{dv}{dt} \right)^2 \right) = \frac{d}{dt} G(v) - \omega \frac{d}{dt} \left(\frac{1}{2} v^2 \right) + \omega u \frac{dv}{dt}.$$

We would like to take the differential operator out of all the terms, but there are still mixed terms of u and v that make this difficult. However, if we take the differential operator out of all the terms where we can, and ignore the mixed terms, we can add both expressions and obtain

$$\frac{d}{dt} \left(\frac{1}{2} \left(\frac{du}{dt} \right)^2 + \frac{1}{2} \alpha \left(\frac{dv}{dt} \right)^2 \right) = \frac{d}{dt} \left(F(u) + G(v) - \frac{\omega}{2} u^2 - \frac{\omega}{2} v^2 \right) + \omega \left(u \frac{dv}{dt} + \frac{du}{dt} v \right).$$

In adding both expressions, the mixed terms add together and form an integrable expression. The expansion is given here:

$$\frac{d}{dt} (\omega u v) = \omega \left(u \frac{dv}{dt} + \frac{du}{dt} v \right)$$

Hence the whole expression under the differential operator can be written as

$$\frac{d}{dt} \left(\frac{1}{2} \left(\frac{du}{dt} \right)^2 + \frac{1}{2} \alpha \left(\frac{dv}{dt} \right)^2 \right) = \frac{d}{dt} \left(F(u) + G(v) - \frac{\omega}{2} u^2 - \frac{\omega}{2} v^2 + \omega uv \right)$$

and if we integrate the expression, and rearrange slightly, we obtain

$$\frac{1}{2} \left(\left(\frac{du}{dt} \right)^2 + \alpha \left(\frac{dv}{dt} \right)^2 \right) = F(u) + G(v) - \frac{\omega}{2} (u - v)^2 + C. \quad (3.39)$$

This equation gives us an expression on the values u , v , du/dt and dv/dt , which are the values we compute solutions of, and relates them to a constant C . This is an energy constant similar to what we derived in the earlier section on the single mass model. Since the constant is unchanging in time, we can use it to verify that a computed solution is reliable by evaluating C at multiple points in the time span of the computation. Figure 3.16 shows an attempted verification of a result using this constant. Due to the nature of the integration method, the energy constant accrues error over the time span of the computation. The computation of the energy constant forms a smooth line, since a small error accrues over the time span of the computation. In this figure, as well as Figures 3.17 and 3.18, we show verification of behaviour through computing the energy constant.

In our computation, even when the tolerances are extremely small, the evaluations of the energy constant will always diverge slightly. This occurs since the error of the numerical method is small but finite, so an error accrues in the energy of the system. Our criterion for a reliable solution is for the energy constant to be exact up to four decimal places. When producing Figures 3.16, 3.17 and 3.18, we have restricted the tolerances such that the solutions meet this criterion, so that we can claim these results are reliable.

3.4.3 The Poincaré map

Because the form of the problem is fourth order, the problem can be analysed as the behaviour of an object in four dimensions. The methods in which we have represented solutions graphically are simplifications, where the four-dimensional behaviour is projected onto a two-dimensional image.

The Poincaré map is a useful technique we can use to analyse the behaviour of a system. First, we construct the Poincaré section, which is an $n - 1$ -dimensional subspace in the space that contains our solutions. Another name for this type of subspace is a *hyperplane*. For a two dimensional problem, the Poincaré section is a line and for our current four dimensional problem it is a three-dimensional space. The Poincaré map is the visualisation of the solution every time it intersects with the Poincaré section. This can be used to assess quasiperiodicity or chaotic nature of dynamical systems.

In our case, we will consider the four dimensional problem as two separate two-dimensional problems, which makes it easier to demonstrate the result. We are essentially reducing the two mass model into two single mass models while acknowledging the coupling between them. For our computations, the respective Poincaré sections for each mass are the lines in the phase portrait where their velocities are zero.

For the case of separate bounded continuous quasiperiodic orbits depicted in Figures 3.12 and 3.18, we can construct the Poincaré map and analyse it in the context of the model. Figure 3.19 visualises the Poincaré map for this problem. We see the intersection points begin to diverge as the computation continues, shown in the visualisations that include the transient. However, these diversions are small and the intersection points are mapped in clearly bounded regions. The diversions shown in the Poincaré map could be attributed to the small but finite numerical error present in the computation.

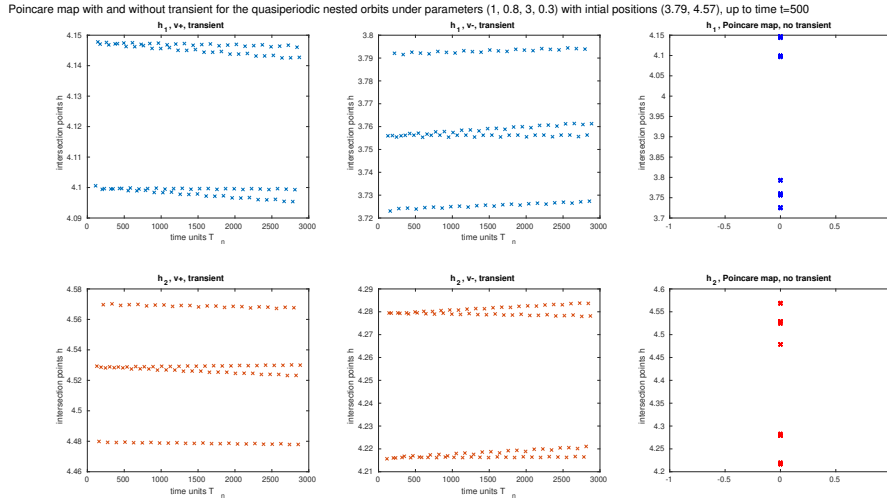


Figure 3.19: The Poincaré map for the orbits represented earlier in Figure 3.12. Parameters (1, 0.8, 3, 0.3) with initial positions (3.79, 4.57). The chosen hyperplane is the respective line where velocity is zero. The first plot is the Poincaré map for h_1 intersecting the line $dh_1/dt = 0$, where $v+$ indicates approaching the line with positive velocity and $v-$ is similar for where velocity is negative. We can identify the intersection regions from the visualisation in the phase portrait in Figure 3.12. The transient is where we have plotted the intersection points against the order in which they were computed.

The method used to compute the Poincaré map [9] constructs a new array of time points T_n of intersections with the Poincaré section, hence the figures do not plot to the same time scale as the original computations.

We have performed a similar computation of the Poincaré map in Figure A.5, for a case we have explored earlier. The points on the Poincaré map are much more irregular and break out of a pattern approximately halfway through the visualised computation. This result is not reliable, justified again by the large scale of change in the energy constant we computed earlier in Figure 3.16.

A regular Poincaré map is a strong indicator that the model exhibits a consistent behaviour, even if that behaviour is extremely complex and difficult to analyse from simpler visualisations.

3.5 Voiced sounds

We can generate playable sound files in .wav format of the time series computations and we can play these back to hear our results. Sound files are generated by interpolating the time series into an array with uniform timestep, normalising the range to $[-1, 1]$ and then using the `audiowrite()` function in MATLAB to write the array to a .wav file. We generate two separate audio files for the motion of each mass. Playable sound files are available here¹, with three results each containing a time series graph we have shown, and two playable sound files for each mass.

¹<https://gitlab.com/willwoolfenden/undergraduate-project-2223-phonation>

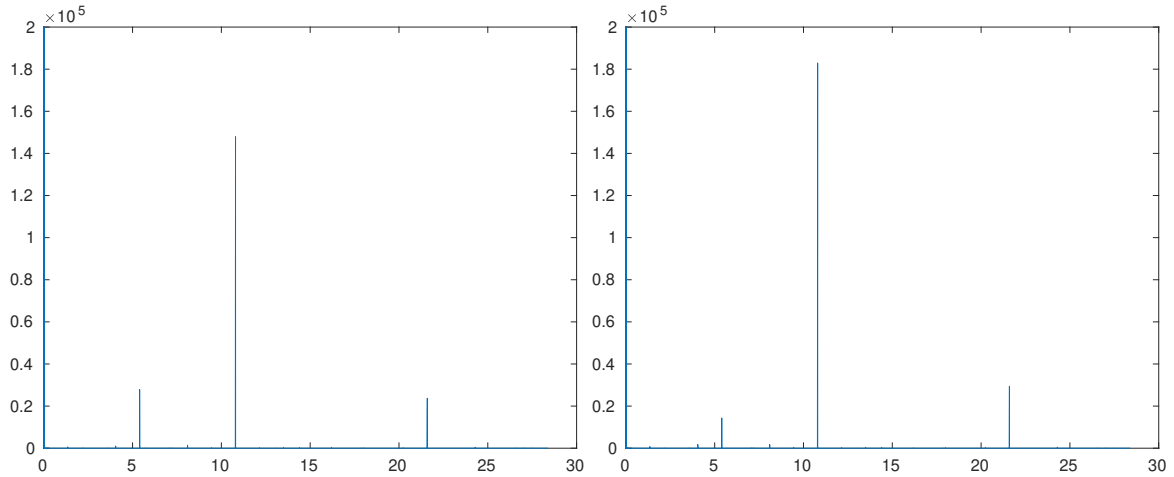


Figure 3.20: Fourier transforms of time series data from same conditions as Figure 3.18, with extended time span. The left figure is the motion of h_1 and the right is h_2 , with parameters $(1, 0.8, 3, 0.3)$ and initial positions $(3.79, 4.57)$. We can identify similar spectra of different magnitude, particularly three distinct spikes with the middle value being the most powerful.

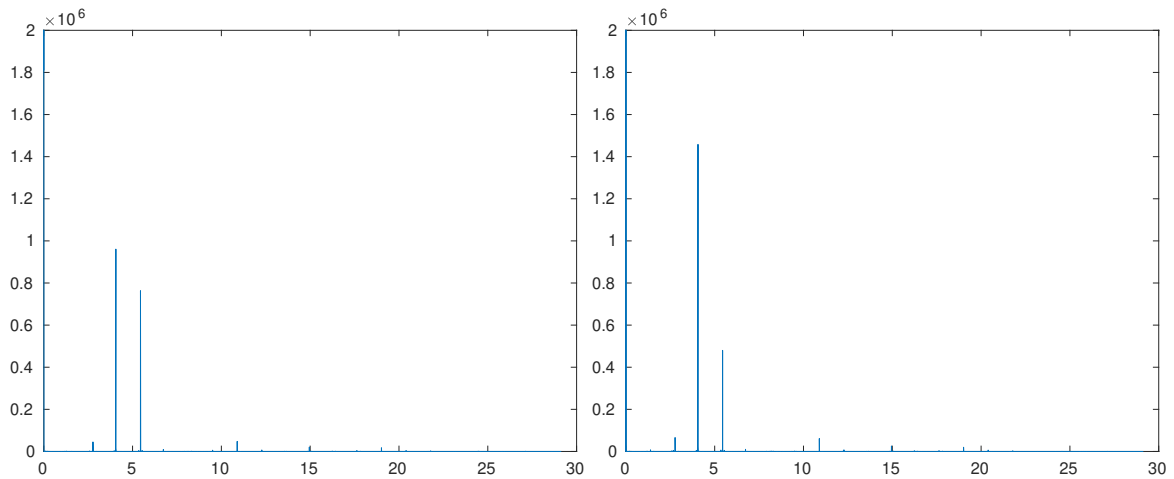


Figure 3.21: Fourier transforms of time series data instead from Figure 3.17, again with extended time span. Presentation is identical to the prior figure. Parameters $(1, 0.8, 3, 0.3)$ and initial positions $(1.80, 3.79)$. The time series of this result shows quasiperiodic orbits with displacement bounds that intersect, as seen in the figure mentioned. The dominant frequencies of oscillation are close together, but the weighting of these frequencies is extremely different in both.

A Fourier transform [10] can be applied to the original time series data to provide information on the frequencies of the oscillations. Figures 3.20, 3.21 and 3.22 apply the transform to data we are familiar with, having extended the time scale. Frequency space is computed as the n points in the time array divided by the total time span. Since the time series data is produced by a non-uniform timestep, we use the `nufft()` function in MATLAB, which is a non-uniform fast Fourier transform

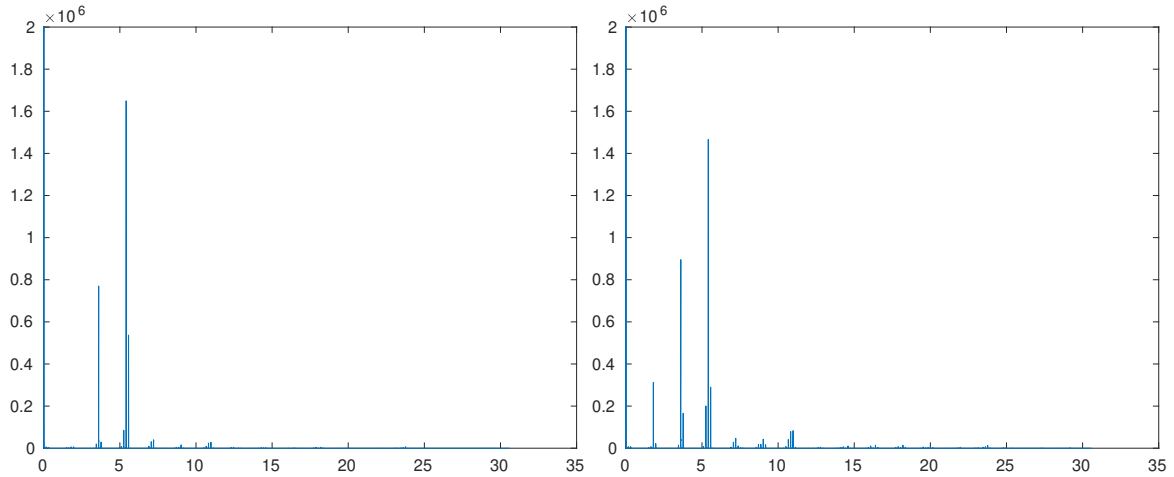


Figure 3.22: Fourier transforms of extended time series data from Figure 3.16. Vertical axis is the power of frequencies on the horizontal. Frequency ranges from 0 to n/T where n is the number of time points and T is the end time of the computation. We computed the solution initialised with parameters $(1, 0.5, 3, 0.3)$ and initial positions $(1, 3.79)$. The continuous quasiperiodic orbits provide a far richer visualisation than the prior two examples, where we can identify clusters of frequencies rather than distinct single spikes of intensity.

algorithm that requires the time series array and the time array as arguments. We apply the Fourier transform to the positions of h_1 and h_2 in the time series.

The frequency domain is not computed by the `nufft()` Fourier transform algorithm, rather it must be computed separately. The domain for frequencies is the sequence $1/T, 2/T, \dots, N/T$, where T is the end time of the computation and N is the number of time points in the array. The entries range from $f = 1/T$, i.e. an oscillation occurs once in the computation, to $f = N/T$, i.e. an oscillation occurs N times in the computation. In practice, $f = N/T$ is impossible in a computation, since N oscillations cannot be stored in N time points. In practice, we tend to only consider the frequencies from $1/T$ to $N/2T$.

On long time scales, solutions may diverge from a consistent behaviour if we do not control the tolerance of the numerical solver. The results provided are computed with the settings `AbsTol` = 10^{-40} and `RelTol` = 10^{-12} . The Fourier transform graphs are all results which have been studied earlier and are all available in the repository.

In all the Fourier transform visualisations we have available, we can identify similar spectra between the masses. Figures 3.20 and 3.21 visualise frequency spectra with discrete spikes. The first plot shows the two masses oscillate with identical frequencies, and the strength of these frequencies are very close in both. In the second, smaller spikes in frequency information do appear more often, which can describe more complex behaviour of the masses. In Figure 3.22, the spectral information is much richer, where frequencies cluster together instead of being distinct spikes. The form of this Fourier transform representation describes much more complex motion of the masses than the other cases we have shown.

3.6 Review

Evidently, a two mass model produces far more insightful results, which reflect the intricate quasiperiodic oscillations that take place in real phonation. We will now conclude our analysis, review potential improvements to our models, and discuss our findings collectively.

Chapter 4

Critique of the models, overview of results and conclusion

4.1 Improving our models

4.1.1 Energy

Both the single mass and the two mass model are systems which perfectly preserve energy. This is not consistent in the computations, but we have shown for both models that there exists a constant term, depending on the variables of position and velocity, which is unchanging in time. From a realistic perspective, systems tend to dissipate energy and eventually come to rest, rather than behaving like perfect conservative machines that operate indefinitely.

Both models we have studied lack any form of damping, so all potential energies are perfectly transferred to kinetic energies and vice versa. If we were to introduce a damping parameter, we would observe closed oscillations about a stationary point to always converge to that equilibrium, rather than oscillating indefinitely.

A mass m attached to a Hooke spring obeys the ODE

$$m \frac{d^2x}{dt^2} + k(x - x_0) = 0$$

where x is the length of the spring, x_0 is the length at rest, k is the stiffness, and t is time. This is the equation for a simple harmonic oscillator, with equilibrium solution $x = x_0$. The general solution is the expression

$$x = x_0 + A \exp\left(\sqrt{-\frac{k}{m}}t\right) + B \exp\left(-\sqrt{-\frac{k}{m}}t\right),$$

where A and B are free constants. With the inclusion of a damping parameter, we obtain a different ODE

$$m \frac{d^2x}{dt^2} + c \frac{dx}{dt} + k(x - x_0) = 0$$

where the constant c describes the damping strength. We retain the equilibrium solution $x = x_0$,

but the general solution changes to

$$x = x_0 + A \exp\left(\frac{-c + \sqrt{c^2 - 4mk}}{2m}t\right) + B \exp\left(\frac{-c - \sqrt{c^2 - 4mk}}{2m}t\right).$$

We require m , k , c to be positive constants. The harmonic oscillator is periodic, whereas the damped harmonic oscillator eventually decays to rest at the equilibrium.

Our models describe systems where energy is perfectly transferred between useful forms, namely potential and kinetic energies. In other words, the systems we study have 100% efficiency. In reality, there are virtually no dynamical systems with this level of efficiency, rather that some energy is always wasted. It would be interesting to develop our models by introducing forms of energy dissipation, such that our models would not describe systems which are 100% efficient. We could then consider how the forcing pressure could adapt to continue phonation to take place when the motion of the vocal cords begins to decay towards equilibrium.

4.1.2 Elasticity

From studies into the material properties of the vocal cords, they have been observed to deform under stress with nonlinear elasticity [1]. However, in the models we have studied, the stiffness of the vocal cords are modelled with linear elasticity by a Hooke spring. It is important to note that in the two mass model, we simplified these assumptions further, by approximating the stiffness coupling by a linear force, rather than as the vertical component of a diagonal spring.

The purpose of our mathematical models are to describe the potentially intricate motion of the vocal cords. In order to do this, we used Hooke springs to model the stiffnesses. While not ideal, these are fundamental to the quasiperiodic behaviours we observed in the two mass model. If we considered non-linear stiffnesses, these might provide fundamentally different oscillations to our observations. However, our analysis does not extend to the impacts of different spring behaviours on the results. Rather, we made the approximation of linear Hooke springs and analysed their impact in depth.

It also serves to mention that the linear Hooke spring is a first-order approximation to the stiffness of a real spring. As such, it is reasonably accurate for small displacements, which occur in the proximity of stable equilibria, being a large portion of our analysis.

4.1.3 Stability of fluid flow

In both models, we applied Bernoulli's equation for a steady flow in order to deduce a relationship between the velocity and the pressure of the fluid. It is possible for the spoken sounds in phonation to be produced by a steady flow, but phonation can occur more generally for unsteady, turbulent flows, and this is not a case which is accommodated in our modelling.

In the two mass model, we forced the assumption of a quasisteady flow, however this reduced the cases we accommodated in the modelling. Ideally we would construct a model which provides accurate simulation of vocal folds moving, subject to a turbulent flow through the glottis. However, the quasisteady flow still provided rich results which led to a wide variety of behaviours which we were able to analyse. Were we to develop the model and introduce the non-steady flow, it would be very important to replicate results from the quasisteady flow assumption. This is because if a model cannot retain a result when a component changes, then there may be something fundamental to that original component, which we have now lost. As such, it was important to focus on the quasisteady flow assumption, even if this does not capture the range of flow types that may be involved in phonation.

When we began to discuss the two mass model, we introduced relationships between the fluxes and the velocities of the masses. We supported these suggestions with the argument of conservation of mass for an incompressible fluid. However, the quasisteady flow was a stronger assumption which neglected these rules. If we were to develop the model, these assumptions on the flux would be good candidates to involve in the modelling. The quasisteady flow implies “change in volume = change in flux” for any fixed volume.

4.1.4 Physical structure of the model

The formulation of the two mass model involved extremely simple geometry, being the flow through a rectangular channel. A more varied and irregular structure, similar to the interior shape of the larynx and glottis, could potentially influence the dynamics of the fluid flow. A varying inner channel width could have implications in Bernoulli flow, and could contribute to more complex flow patterns in phonation.

The masses which model the vocal cord are extremely simple objects, being stiffness-coupled planes, and are restricted to one dimensional motion in the direction of their outward normal. In reality, the vocal folds have a much more intricate shape than the cuboid blocks we modelled them as. We could develop the two mass model by constructing the vocal fold with a much more geometrically complex shape, and allowing more degrees of freedom in their motion. This would lead to more complex behaviour in the motion of the masses, but it would be difficult to recover results from the simpler model which we have analysed. This is because the ODE we have analysed in the two mass model is characteristic of the one dimensional motion. If we were to remove this restriction, we would obtain a system of PDEs describing motion in more than one degree of freedom, and it would be difficult to replicate the one dimensional results from our two mass model.

4.2 Discussion

4.2.1 Aims

In this project, we aimed to explore mathematical models for phonation, and analyse the characteristics that they can produce. We began by exploring a single mass model from a research paper, and derived results on its behaviour. We explored equilibrium solutions and criteria for closure.

We generalised the properties of the single mass problem into a model involving two separate, stiffness-coupled masses. We analysed distinct behaviours of the two mass model, again investigating equilibrium solutions. We investigated the complex shape of the motion of the masses, and performed computational Fourier analysis on different results to provide insight into the frequencies of the oscillations.

4.2.2 The single mass model

The single mass model exhibits oscillations when parameters take suitable values. Orbits oscillate about a stable equilibrium b_2 in the phase portrait. In the proximity of the unstable equilibrium b_1 , orbits will gravitate towards the unstable point. Trajectories near b_1 outside the bound for oscillations will diverge from this unstable point and eventually reach closure.

4.2.3 The two mass model

We constructed the two mass model by generalising the single mass model, but we chose to cover the formulation of the model from scratch. Two masses are given a coupling stiffness, and we aim to produce more complex dynamics with the two mass model.

The two mass model always retains at least one equilibrium solution. Strong stiffness coupling between the masses can replicate the structure of solutions for the single mass model. In most cases, we can observe four separate equilibrium solutions for the system. Results such as the equilibrium solutions themselves, and the eigenvalues of the Jacobian local to these points, must be computed numerically. Some equilibrium solutions are often unstable and so precise that a computation at these equilibria eventually diverges into large oscillations. The motion of the masses is often quasiperiodic, following one or several dominant frequencies of oscillation.

We could verify results by deriving an energy constant for the system from definite integration. This energy constant was used to verify the reliability of results.

Finally, we performed Fourier analysis on a selection of results in order to analyse the frequency space of the quasiperiodic motion. We were able to analyse the spectra of the oscillations, where some results showed clear discrete peaks in the frequency space, but others showed more continuous ranges of oscillation frequencies.

4.2.4 Equilibrium solutions

The existence of equilibrium solutions suggests that, during phonation, the vocal folds can remain in fixed positions under particular forcing terms. The nature of stable and unstable equilibria imply different relationships between forces local to these points. An unstable equilibrium suggests that a vocal cord may remain in a fixed shape under a precise balance of forces, and will diverge from this position when offset even slightly. However, a stable equilibrium implies that if energy were to slowly dissipate from the system then a vocal cord will come to rest at a fixed position.

The two mass model yields different kinds of equilibrium solutions. We defined two categories, being diagonal and off-diagonal equilibria. The diagonal equilibria are stationary points where both components of a vocal cord are close together. When a diagonal equilibrium is unstable, the components of the vocal cord start close together but are sensitive to initial conditions, and if their positions are offset slightly then they will diverge into their own quasiperiodic motions like we observed. If the point is instead stable then a slight offset leads to continuous small oscillations. The off-diagonal equilibria are points where the components of a vocal cord have a significant distance apart from each other, so the stiffness coupling induces tension which is balanced by the Bernoulli flow and individual stiffnesses. We have no results where the off-diagonal equilibria are stable, instead we have observed that the component positions diverge when slightly offset. In fact, these are so sensitive to position that the machine arithmetic used in our computations is not precise enough to store variables that maintain equilibrium. The eigenvalues of these equilibria are entirely imaginary in all cases we have considered.

4.2.5 Quasiperiodic motion

We analysed the Fourier spectrum of the motion of the two mass model, showing that the motions are formed from a harmonic series of frequencies. Different Fourier spectra indicate different combinations of the harmonic series, which produce different textures of sound. This analysis applies most naturally to pitched sounds, such as the tones produced by musical instruments. If, for example, we recorded a violin and a clarinet both playing exactly the same note and performed Fourier transforms on the data, we would observe vastly different frequency spectra with the same fundamental

frequency. Singing is an example of phonation producing pitched sounds, however natural speech also has pitch and timbre formed from a harmonic series. Hence, we can apply the Fourier transform to analyse the frequency spectrum. From our results, we deduced that the two mass model is capable of producing a range of sound textures from the range of unique frequency spectra we observed.

4.2.6 Collapse

The collapse of the glottis in regular phonation leads to the airway becoming blocked and building up pressure. In our analysis, however, closure is considered to be a stopping condition and hence we do not explore behaviours after collapse. The single mass model accommodated for the possibility of no equilibrium solutions, and in these cases we would always observe closure in sufficient time. For the two mass model, there is instead always at least one equilibrium solution, so we do not have the same closure conditions. However in both of our models, collapse tends to occur when either one or both masses is sufficiently close to 0, where the Bernoulli pressure term in the model dominates and the masses accelerate to closure.

These results could infer that in real phonation, a sufficiently small glottal opening could cause collapse, and so the oscillations can only be sustained if they remain bounded to a particular interval. If the range of oscillations is too large and exceeds these bounds, the glottal opening could become too small would cause a dominating pressure term, where it would be likely for closure to occur.

4.3 Conclusion

From our models, we can deduce that the principle factors in phonation are the stiffness of the vocal cords and how they behave under the pressure from a steady Bernoulli flow from the lungs. A two mass model characterises phonation as the motion of two stiffness-coupled components of a single vocal fold. Under sufficient parameters, the two mass model reproduces the regular periodic orbits that we see in the single mass model. However, the two mass model is much more sensitive and shows more interesting behaviours, since it is a fourth order system describing two masses with a stiffness coupling. In general, we observe quasiperiodic motion of the components of the vocal folds, and the model accommodates that oscillations could continue indefinitely due to the lack of any energy sink in the model. This quasiperiodic motion is a weighted sum of a harmonic series of frequencies, which can be visualised using a Fourier transform. The two mass model is capable of producing signals with discrete peaks in the frequency spectrum, but also with frequencies clustered together more continuously. In the results we have observed, both components of the two mass model appear to resonate with each other, since the frequency domains are often identical but the power representations in the Fourier transforms are weighted slightly differently.

We have discussed approaches which could improve the model. To extend the study of models for phonation, we could apply a more complex circulation of energy within the system. We could also consider more kinds of fluid flow, for example by exploring how phonation may occur for turbulent, unstable flows. In turn, it could be beneficial to develop the geometry of our models, and consider multiple degrees of freedom in the motion of the modelled vocal folds. Were we to develop these aspects of our model, it would be interesting to see how our results develop, however it is also important that we are still able to reproduce fundamental results.

The two mass model we have studied is capable of producing quasiperiodic motions of two stiffness-coupled components of a vocal cord. In formulating the model, we have made assumptions that may limit the potential for valuable, intricate results that provide strong insight into the nature of phonation. However, the results we have obtained provide forms of motion which we can analyse

and relate to real phonation. Particularly, we showed that the results from the two mass model can be analysed as a harmonic series of frequencies, which is a key characteristic of the acoustic structure of voiced sounds.

Bibliography

- [1] Fariborz Alipour and Sarah Vigmostad. Measurement of vocal folds elastic properties for continuum modeling. *Journal of Voice*, 26(6):816–e21, 2012.
- [2] Kenzo Ishizaka and James L. Flanagan. Synthesis of voiced sounds from a two-mass model of the vocal cords. *Bell System Technical Journal*, 51(6):1233–1268, 1972.
- [3] Ingo R. Titze. Comments on the myoelastic-aerodynamic theory of phonation. *Journal of Speech, Language, and Hearing Research*, 23(3):495–510, 1980.
- [4] Noam J. Gavriely and Oliver E. Jensen. Theory and measurements of snores. *Journal of Applied Physiology*, 74(6):2828–2837, 1993.
- [5] Peter Birkholz, Bernd J. Kröger, and Christiane Neuschaefer-Rube. Synthesis of breathy, normal, and pressed phonation using a two-mass model with a triangular glottis. In *Twelfth Annual Conference of the International Speech Communication Association*, 2011.
- [6] Lawrence Perko. *Differential equations and dynamical systems*. Texts in applied mathematics ; 7. Springer, New York, 2nd edition, 1996.
- [7] Lawrence F. Shampine and Mark W Reichelt. The matlab ode suite. *SIAM Journal on Scientific Computing*, 18(1):12–13, 1997.
- [8] Cleve B. Moler. Ordinary differential equation solvers ode23 and ode45. <https://blogs.mathworks.com/cleve/2014/05/26/ordinary-differential-equation-solvers-ode23-and-ode45/>, 2014.
- [9] Sanjay G. Manohar. poincare map. https://www.mathworks.com/matlabcentral/fileexchange/72506-poincare_map, 2011.
- [10] Artyom M Grigoryan and Merughan Grigoryan. *Brief Notes in Advanced DSP: Fourier Analysis with MATLAB*.

Appendix A

Computations

A.1 Unstable results

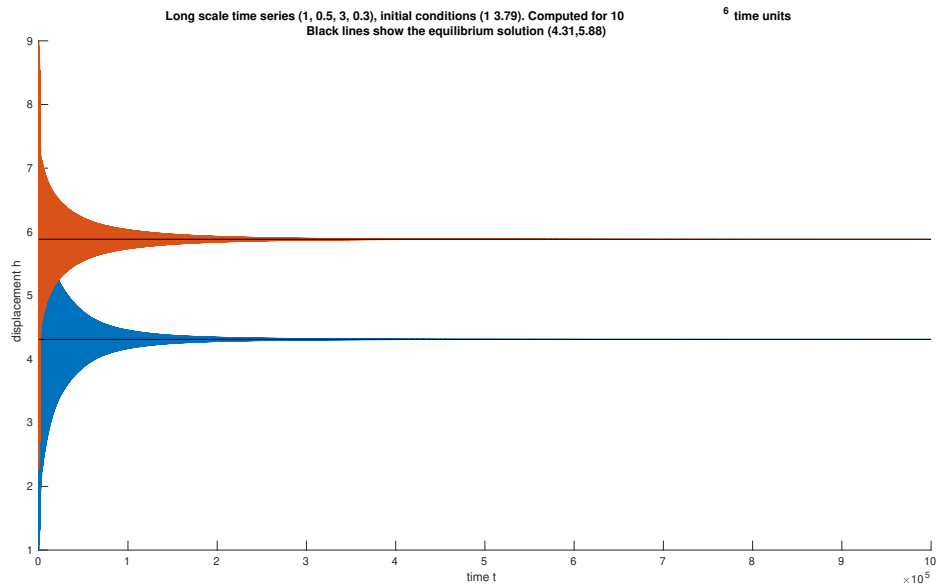


Figure A.1: Long term behaviour of the model under parameters $\alpha = 1$, $\lambda = 0.5$, $\beta = 3$, $\omega = 0.3$. Computed with `ode45()` using default tolerances. Oscillations tend towards an equilibrium solution given computation on a large timescale. Initial conditions $(1, 3.79)$. The equilibrium solution is computed to be $(4.31, 5.88)$. The behaviours diverge from the initial behaviours and slowly settle to equilibria, despite the lack of any damping in the system. This is an unreliable solution, due to an inadequately high tolerance in the computation.

We cannot expect a numerical method to produce results which would perfectly match analytical behaviours. However, it is sensible to deduce that there are families of behaviours that the model may exhibit, which the numerical methods are incapable of reproducing. For example, the

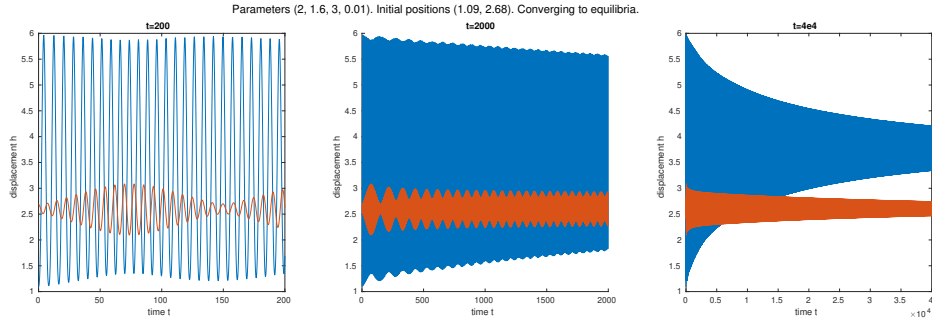


Figure A.2: Parameters given are $(1, 0.8, 3, 1)$. The masses oscillate near independently starting at different positions $(1.96, 0.83)$ at time $t = 0$. The figures, left to right, progressively increase the time we run the computation. We can see in the left-most plot that the weak coupling leads to the masses oscillating at independent frequencies. As running time increases, the masses converge to their own equilibrium positions.

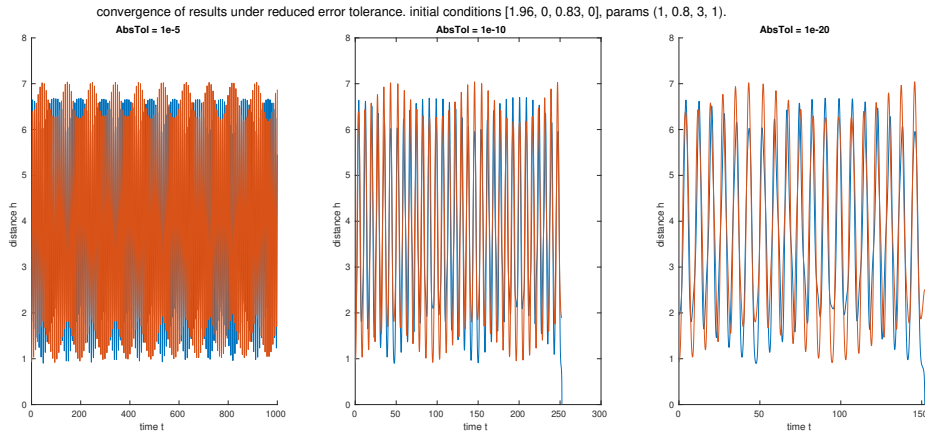


Figure A.3: Changes in solution as `AbsTol` is decreased. Computations under parameters $(1, 0.8, 3, 1)$ with initial positions $(1.96, 0.83)$. The computed solution fundamentally changes under stepping down the tolerance.

computation shows that the initial quasiperiodic behaviour of Figure 3.14, which eventually settles to the stable equilibrium as shown in Figure A.1, can be shown to be invalid through computing the energy constant shown in Figure 3.16. Since the computation of the energy constant for this problem progressively decreases, we could guess that the quasiperiodic motions will instead continue indefinitely as shown in the early region of the time series.

The numerical solver struggles with the unstable equilibrium solutions, since near these points, the ODE is extremely sensitive to minute differences in the numerical values. Due to finite precision floating point arithmetic, it is extremely difficult to produce consistent results near the unstable equilibria numerically. In combination with the stiffness coupling, there are often heavily unbalanced forces on each mass, for example if an unstable equilibrium lies between the two masses. Figures A.4 and A.5 show analysis of computations where the behaviour has diverged from a consistent result.

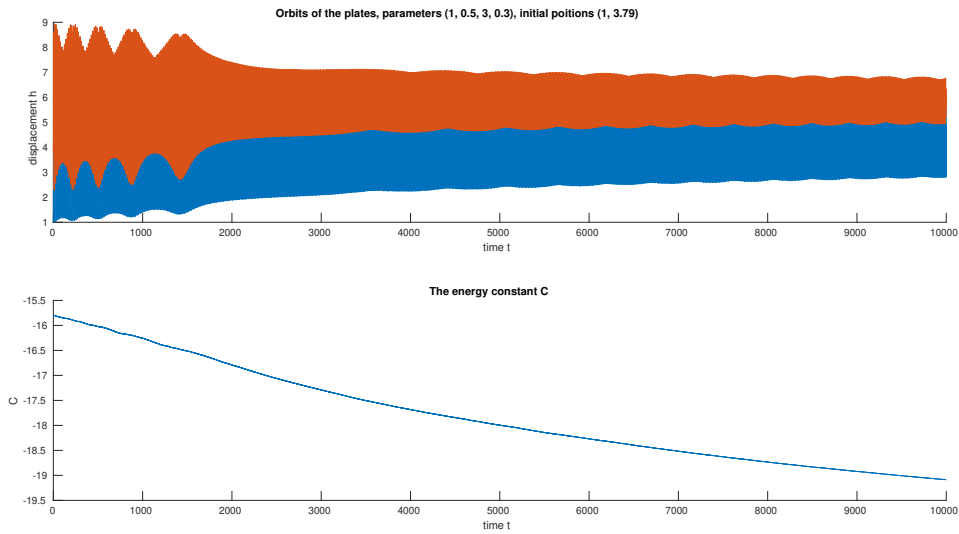


Figure A.4: Solution from `ode45()` for the problem seen in Figures 3.14 and 3.16. Without reducing the tolerance of the solver, the solution diverges.

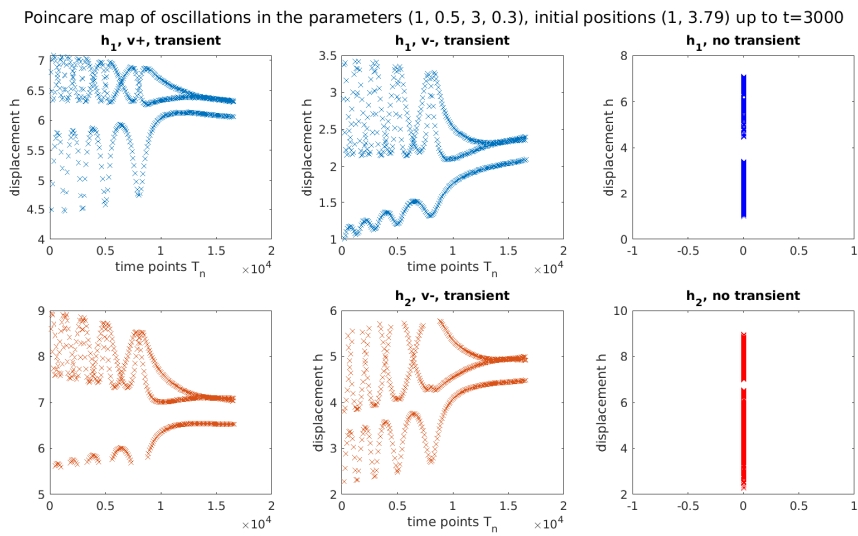


Figure A.5: Another example of the Poincaré map, for the computation shown earlier in Figure A.1. We have shown that this result is not reliable, since we can compute that the energy constant diverges. As we can see, the orbits break out of a pattern and the points on the Poincaré map begin to converge.

The time series slowly breaks out of quasiperiodic orbits and begins to converge towards a stable

equilibrium, while the reliable solution in Figure 3.16 shows continuous quasiperiodic behaviour.

Figure A.3 shows a change in results when reducing the `AbsTol` parameter for the MATLAB `ode45()` function. The figures show that decreasing the error tolerance can fundamentally change the numerical solution, especially where closure is not observed for tolerance of order 10^{-5} , but is observed for 10^{-10} . Recall that `AbsTol` is a lower bound on the magnitude of the solution that MATLAB will compute. Clearly, the closure of the model, being the case of a mass approaching zero, is affected by how MATLAB handles solutions that approach zero.

Appendix B

MATLAB Scripts

B.1 Single mass model

This code produces computations of the single mass model. It also includes plotting functions for the curves which represent trajectories in the phase portrait.

```
%% ODE Solver using ode45

tspan=[0,20];

%initial conditions. this field should be edited for new results
xinit=[0.2, 0];

q=0.1; k=0.1;
mu = 1;
[t, x] = ode45(@(t,x) OscODE(t,x,mu,q), tspan, xinit)
b=x(:,1);
bdot=x(:,2);

%plot the computation
hold on
plot(t,b)
hold off

%compute equilibrium solutions and store
b_1 = fzero(@(b) OscODE2(t,b,mu,q),0.4)
b_2 = fzero(@(b) OscODE2(t,b,mu,q),0.6)

%% KE Curves Plotter

hold on

fplot(@(x) sqrt(F(x,mu,q) - F(b_1,mu,q)), [0 2])
fplot(@(x) sqrt(F(x,mu,q) - F(b_2,mu,q)), [0 2])
```

```

fplot(@(x) sqrt(F(x,mu,q) + F(b_1,mu,q)), [0 2])
fplot(@(x) sqrt(F(x,mu,q) + F(b_2,mu,q)), [0 2])

fplot(@(x) sqrt(F(x,mu,q) - (F(b_2,mu,q) - F(b_1,mu,q))), [0 2])
fplot(@(x) sqrt(F(x,mu,q) - (F(b_2,mu,q) + F(b_1,mu,q))), [0 2])

fplot(0,[0 2], 'k-')
hold off

%% Functions

function dbdt = OscODE(t, x, mu, q)

b=x(1);
bdot=x(2);

dbdt=zeros(size(x));
dbdt(1) = bdot;
dbdt(2) = 1 - q - b - (mu*power(q,2))/(2*power(b,2));

end

function d2b = OscODE2(t, b, mu, q)
% used for computing equilibria

d2b = 1 - q - b - (mu.*power(q,2))/(2*power(b,2));

end

function out = F(b,mu,q)
out = (1-q)*b - (b^2)/2 + (mu*q^2)/(2*b);
end

```

B.2 Two mass model

This is the code used to compute results for the two mass model. Should be run separately by section. For a quick result, run the first section, then “stationary points and general equilibria solvers”, then the implementation of `ode45`. Also includes code for computing eigenvalues near an equilibrium, plotting graphics of the equilibrium solutions, and extra functions for verification and computation.

```

%% Two Mass Model - Normalised ODE Attempt 3

% final nondimensionalisation

%set the required constants

```

```

% alpha is quotient of second mass by first mass, we specify only its
% inverse alpha_inv = m1/m2 since we only ever divide by alpha.
% lambda is the quotient of their support spring stiffnesses k2/k1.
% beta is proportional to the forcing pressure at lung.
% omega is the quotient of the coupling stiffness by spring 1, i.e. if we
% know omega and lambda, you can find the stiffness k_2.

alpha_inv = 1;
lambda = 0.8;
beta = 3;
omega = 0.3;

%% Stationary points and general equilibria solvers

%one-dimensional solvers for individual stationary points, neglecting the
%stiffness coupling
stat_point_11 = fzero(@(x) 1 - x + beta*(1 - power(x, -2)),[1e-5 power(2*beta, 1/3)]);
stat_point_12 = fzero(@(x) 1 - x + beta*(1 - power(x, -2)),[power(2*beta, 1/3), 10]);
stat_point_21 = fzero(@(x) lambda*(1 - x) + beta*(1 - power(x, -2)),[1e-5 power(2*beta/lambda, 1/3), 10]);
stat_point_22 = fzero(@(x) lambda*(1 - x) + beta*(1 - power(x, -2)),[power(2*beta, 1/3), 10]);

%solver problem to find equilibria. MUST take vertical vector input
init_search_point = [stat_point_12; stat_point_22];
[steady_soln,fval] = fsolve(@(v) zeroesFunction2(v,lambda,beta,omega),init_search_point);

x_equilibrium = steady_soln(1);
y_equilibrium = steady_soln(2);

%% Eigenvalue computation

df1dx = partDf1(x_equilibrium,beta,omega);
df1dy = omega;
df2dx = omega;
df2dy = partDf2(y_equilibrium,lambda,beta,omega);

jcbn = [
0, 1, 0, 0;
df1dx, 0, df1dy, 0;
0, 0, 0, 1;
alpha_inv*df2dx, 0, alpha_inv*df2dy, 0;
];

eig_vals = eig(jcbn)

% plot the eigenvalues in the complex plane with real, imag axes
hold on
for val = eig_vals
plot([-5 5],[0 0],'k-')

```

```

plot([0 0],[ -5 5], 'k-')
plot(real(val),imag(val), 'rx', 'MarkerSize',8)
end
hold off

%% Contour graphic of equilibrium solutions

x_axis = [-5:0.05:15];
y_axis = [-5:0.05:15]';
z_axis_1 = 1 - x_axis + beta*(1-1./(x_axis.^2)) + omega*(y_axis-x_axis);
z_axis_2 = lambda*(1 - y_axis) + beta*(1-1./(y_axis.^2)) + omega*(x_axis-y_axis);

hold on
contour(x_axis,y_axis,z_axis_1,[-0.001,0,0.001], 'b-')
contour(x_axis,y_axis,z_axis_2,[-0.001,0,0.001], 'r-')
plot([-5 15],[-5 15], 'g-')
hold off

%% Solver - Implementation of ODE45

%enter initial conditions
opts = odeset('AbsTol',1e-20,'RelTol',1e-12);
tspan = [0 100];
init = [stat_point_12, 0, stat_point_22, 0];
[t,x] = ode45(@(t,x) twoMassModel(t,x,alpha_inv, lambda, beta, omega),tspan,init,opts);

E = totalEnergy(x(:,1),x(:,2),x(:,3),x(:,4),alpha_inv,lambda,beta,omega);

% plot different representations
hold on
%plot(x(:,1), x(:,2), 'b');
%plot(x(:,3), x(:,4), 'r');

plot(t, x(:,1))
plot(t, x(:,3))

%plot(t,E)

%plot(x(:,1),x(:,3))
%hold off

%% Les fonctiones

%the ODE function on two masses taking parameters alpha, lambda, beta,
%omega
function dhdt = twoMassModel(t,x,alpha_inv,lambda,beta,omega)

%take inputs, initialise the h variables

```

```

dhdt = zeros(size(x));

h_1 = x(1);
dh_1 = x(2);
h_2 = x(3);
dh_2 = x(4);

%compute the equation

dhdt(1) = dh_1;
dhdt(2) = 1 - h_1 + beta*(1-1/(h_1)^2) + omega*(h_2-h_1);
dhdt(3) = dh_2;
dhdt(4) = alpha_inv*(lambda*(1 - h_2) + beta*(1-1/(h_2)^2) + omega*(h_1-h_2));

end

function out_vector = zeroesFunction2(v,lambda,beta,omega)
x = v(1);
y = v(2);
out_x = 1-x + beta*(1-(1./(x.^2))) + omega.*(y-x);
out_y = lambda*(1-y) + beta*(1-(1./(y.^2))) + omega.*(x-y);
out_vector = [out_x; out_y];
end

%partial derivatives of f1 and f2
function out = partDf1(x,beta,omega)
out = -1 + 2*beta*power(x,-3) - omega;
end
function out = partDf2(x,lambda,beta,omega)
out = -lambda + 2*beta*power(x,-3) - omega;
end

% conserved energy term
function vec = totalEnergy(x1,v1,x2,v2,alpha_inv,lambda,beta,omega)
kinetic_energy_term = (v1.^2 + (alpha_inv^-1)*(v2.^2))/2;
x_potential_term = (1+beta)*x1 - (x1.^2)/2 + beta./x1;
y_potential_term = (lambda+beta)*x2 - lambda*(x2.^2)/2 + beta./x2;
mixed_term = -omega*((x1-x2).^2)/2;
vec = kinetic_energy_term - x_potential_term - y_potential_term - mixed_term;
end

function starting_pts = findStatPoints(lambda,beta)
stat_point_11 = fzero(@(x) 1 - x + beta*(1 - power(x, -2)),[1e-5 power(2*beta, 1/3)]);
stat_point_12 = fzero(@(x) 1 - x + beta*(1 - power(x, -2)),[power(2*beta, 1/3), 10]);
stat_point_21 = fzero(@(x) lambda*(1 - x) + beta*(1 - power(x, -2)),[1e-5 power(2*beta/lambda, 1/3), 10]);
stat_point_22 = fzero(@(x) lambda*(1 - x) + beta*(1 - power(x, -2)),[power(2*beta, 1/3), 10]);

```

```

starting_pts = [
stat_point_11, stat_point_12;
stat_point_21, stat_point_22
];
end

function [equilibria_x,equilibria_y] = findEquilibria(sp11,sp12,sp21,sp22,lambda,beta,omega)
%opts_2 = optimset()
steady_soln_11 = fsolve(@(v) zeroesFunction2(v,lambda,beta,omega), [sp11,sp21]);
steady_soln_12 = fsolve(@(v) zeroesFunction2(v,lambda,beta,omega), [sp11,sp22]);
steady_soln_21 = fsolve(@(v) zeroesFunction2(v,lambda,beta,omega), [sp12,sp21]);
steady_soln_22 = fsolve(@(v) zeroesFunction2(v,lambda,beta,omega), [sp12,sp22]);
if any([steady_soln_11 steady_soln_12 steady_soln_21 steady_soln_22]<0)
equilibria_x = [
missing missing;
missing missing
];
equilibria_y = [
missing missing;
missing missing
];
end
equilibria_x = [
steady_soln_11(1), steady_soln_12(1);
steady_soln_21(1), steady_soln_22(1)
];
equilibria_y = [
steady_soln_11(2), steady_soln_12(2);
steady_soln_21(2), steady_soln_22(2)
];
end

```

B.3 Fourier transform and sound file generation

This code requires that a computation of the two mass model has been performed and is currently stored.

```
%% Sound System
```

```
%Generates a playable wave form and a Fourier spectrum from data provided
%by the vocal fold model.
```

```
%use nufft() for fourier transform
```

```
%fourier analysis
```

```
D1 = x(:,1);
D2 = x(:,3);
N = length(t);
```

```

L = t(N);
F = (0:N-1)/L;

%fourier transform
M1 = nufft(D1, t);
M2 = nufft(D2, t);

%conversion to the power of the frequencies
P1 = abs(M1.^2)/N;
P2 = abs(M2.^2)/N;

%% Generate Sound Files

%reinterpolate the signal to a uniform step
t_new = linspace(0,L,N);
V1 = interp1(t,D1,t_new);
V2 = interp1(t,D2,t_new);

%normalise the signal to [-1, 1]
signal_u = max(max(V1),max(V2));
signal_l = min(min(V1),min(V2));

translation = -(signal_u+signal_l)/2
scaling = 2/(signal_u-signal_l)

V1 = scaling*(V1+translation);
V2 = scaling*(V2+translation);

%suggested playback frequency. 1000 time units is one second
playback_frequency = floor(1000*N/L)

filename="result_name";
info = "parameters alpha=%d, lambda=%d, beta = %d, omega = %d. IV [%d %d]";
comment = sprintf(info,1/alpha_inv,lambda,beta,omega,init(1),init(3));
audiowrite(filename+"a.wav",V1,playback_frequency,'Comment',comment);
audiowrite(filename+"b.wav",V2,playback_frequency,'Comment',comment);
figure1 = plot(F,P1); ylim([0 2e5]); saveas(figure1,filename+"a",'epsc');
figure2 = plot(F,P2); ylim([0 2e5]); saveas(figure2,filename+"b",'epsc');

```